



Original Paper

San Felipe Geothermal Prospect: A Previously Unrecognized Hydrothermal System on the Northeastern Coast of the Baja California Peninsula, México

R. M. Prol-Ledesma^{1,4}, A. A. Rodríguez-Díaz,¹ C. E. González-Idárraga,²
I. A. González-Romo,¹ A. S. Membrillo-Abad,³ M. Errasti,³ and M. A. Torres-Vera³

Received 20 April 2023; accepted 4 October 2023
Published online: 2 November 2023

Geophysical surveys discovered low resistivity values that, in combination with geochemical and structural data, indicate the presence of a previously unrecognized geothermal system with a possible maximum size potential similar to that of the presently installed capacity of the Cerro Prieto geothermal field. The only evidence of a hydrothermal system in the San Felipe Valley are warm groundwater wells and four intertidal hot springs. Exploration at San Felipe was part of a research project that included geological, geochemical and geophysical studies, which indicated the presence of low resistivity anomalies and high temperature at depth; the geological survey provided evidence of active fault systems that may act as channels for convective heat transport. Estimation of the energy potential of the San Felipe prospect using the heat in place method yielded a 50% probability of more than 300 MW that would add to the 570 MW of the Cerro Prieto geothermal field and can supply almost 40% of the state of Baja California electricity demand. The Baja California Peninsula is not connected with the national grid and has one of the highest electricity prices in Mexico, which should be an incentive to develop this clean energy source. The results of this work support the recommendation to pursue further advanced exploration of this prospect.

KEY WORDS: Geothermal system, Heat in place, Intertidal vents, Gulf of California.

INTRODUCTION

The Baja California Peninsula (BCP) hosts the third largest geothermal field in the world—Cerro Prieto (570 MW installed capacity)—and it hosts a large number of geothermal systems that might be

exploited (Arango-Galván et al., 2015). Economic development in this region has triggered an increase in energy demand, as nowadays almost five million people live there. The present average electricity demand in BCP is approximately 2,000 MW (CENACE, <https://www.cenace.gob.mx/GraficaDemanda.aspx>) and a large part of it could be produced by clean energy sources. In 2013, an increase in clean energy production was expected (Quintero-Núñez et al., 2013) based on the vast renewable energy resources of the BCP; however, the present energy policies of the government favor the construction of new fossil fuel plants and the BCP energy expansion plans include only fossil energy sources: four gas units to produce 138 MW and the

¹Departamento de Recursos Naturales, Instituto de Geofísica, Universidad Nacional Autónoma de México, Circuito interior s/n, Coyoacán, 04510 Mexico City, Mexico.

²Posgrado en Ciencias de la Tierra, Universidad Nacional Autónoma de México, UNAM, Mexico City, Mexico.

³Facultad de Ingeniería, Universidad Nacional Autónoma de México, UNAM, Mexico City, Mexico.

⁴To whom correspondence should be addressed; e-mail: prol@igeofisica.unam.mx

construction of a new 250 MW combined cycle plant. Previous evaluations have shown the enormous clean energy potential of the BCP with abundant solar, wind, tidal, ocean thermal gradient, ocean currents, and particularly geothermal energy; therefore, future energy projections should include an important increase in clean energy production (Popkin, 1982; Muñoz-Meléndez et al., 2012; Arango-Galván et al., 2015; Magar et al., 2020; Muñoz-Andrade et al., 2020).

The northern part of the BCP hosts numerous geothermal areas in the Mexicali Valley and along the coast of the Gulf of California (Arango-Galván et al., 2015), many of which present limited or no surface manifestations due to the arid climate in the region. Therefore, the study of groundwater wells provides important clues to locate those previously unrecognized geothermal systems. One of these geothermal areas is San Felipe (Fig. 1), located to the south of Mexicali, where there are reports of warm water wells in the valley and after reconnaissance work some intertidal thermal springs were found (Portugal et al., 2000; Barragán et al., 2001; Arango et al., 2015). Moreover, a magnetotelluric (MT) survey intended to study the tectonic evolution of the region resulted in the discovery of low resistivity anomalies to the north of San Felipe and attracted attention to this area (Pamplona-Pérez, 2007). However, until now San Felipe geothermal prospect has been disregarded and no integrated exploration project had been undertaken to evaluate its potential. Here, we present new geological and geochemical data, MT data reprocessing, and their integration with previously reported information to estimate the geothermal potential of this area as a contribution to the quantitative indication of the entailed clean energy sources to comply with Baja California's future energy demand.

GEOSCIENTIFIC INFORMATION OF THE STUDY AREA

Geological Setting and Hydrothermal Manifestations

The most relevant tectonic processes in this area correspond to the opening of the Gulf of California that followed the cessation of subduction west of the current Baja California Peninsula at ca. 12–15 Ma (Atwater & Stock, 1998; Mark et al., 2017). The middle to late Cenozoic extension in

central and western Mexico formed the Basin and Range province with its western branch that extends along the eastern coast of Baja California (Fig. 1) and it is called the Gulf Extensional Province (Gastil et al., 1975; Henry & Aranda-Gómez, 2000). The Main Gulf Escarpment is considered a break-away fault of the continental rifting in the Gulf Extensional Province (Gastil et al., 1975; Seiler et al., 2010). The extension stretched westward behind the subduction-related Paleogene to Neogene volcanic arc, currently dissected by the Gulf of California (Scott et al., 2014). The opening of the Gulf of California is the result of oblique extension between the Pacific Plate and the North American plate; transtensional shearing motion is currently accommodated by a NNW-trending system of right-stepping, en echelon, strike-slip and oblique slip faults related to pull-apart basins or spreading centers (Atwater & Stock, 1998; Scott et al., 2014; Mark et al., 2017).

The San Felipe region is located within the Gulf Extensional Province of northeastern BCP and it hosts normal faults, block rotations and extensional-parallel folding that show a history of complex deformation related to the opening of the Gulf of California (e.g., Seiler et al., 2010; Fig. 1). The main regional structure in the San Felipe area is the San Pedro Mártir Fault, which is part of the Main Gulf Escarpment fault zone and it consists of an active NNW-trending normal fault with listric geometry at depth, which produces a 1000–2500 m high topographic escarpment that extends ~100 km along strike and that separates the batholith of Sierra San Pedro Mártir from Sierra San Felipe and Valle Chico (Seiler et al. 2010). Two major dextral strike-slip faults, Agua Blanca and San Miguel (Wetmore et al., 2019), converge with the San Pedro Mártir Fault on the western edge of the San Felipe area (Fig. 1). The San Miguel and Vallecitos fault systems, farther north, are the most active structures in the region that have produced moderate earthquakes with magnitudes of up to 6 (Gutiérrez-Gutiérrez & Suárez-Vidal, 1988). Suárez-Vidal et al. (1991) and SGM (1999) suggested that the Agua Blanca and San Miguel faults continue through the BCP down to the coast near San Felipe.

The range-front of the Sierra San Felipe and Santa Rosa is defined by three left-stepping, en echelon detachment faults that are linked by dextral and sinistral transfer faults (Seiler et al., 2010). The Las Cuevitas, Santa Rosa and Huatamote detachments comprise NE- to SE-dipping, moderate- to

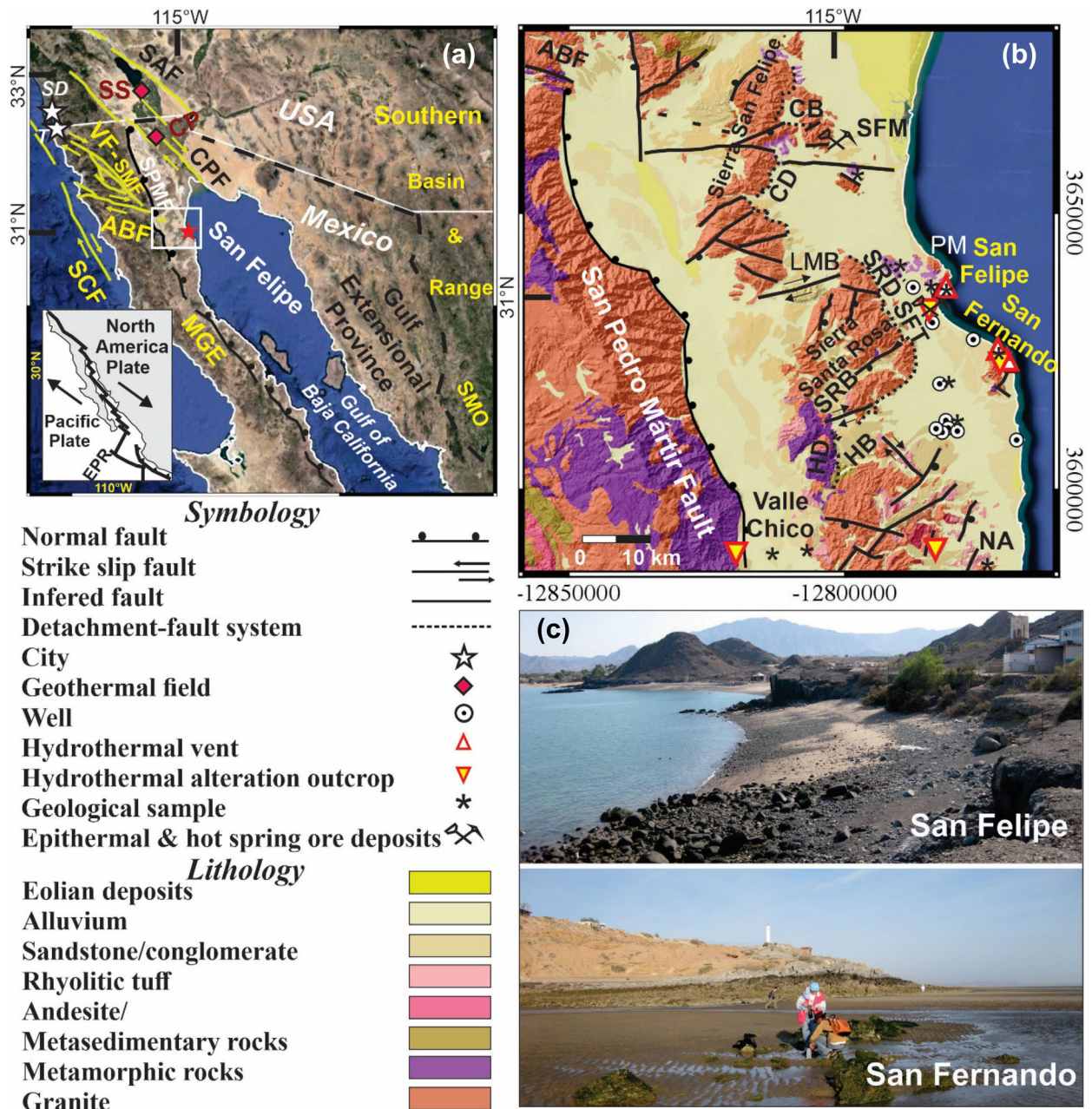


Figure 1. (a) Regional map of northern of Baja California Peninsula with the main structural features (simplified after Gastil et al., 1975; Suárez-Vidal et al. 1991; Henry & Aranda-Gómez, 2000; Oskin & Stock 2003a). (b) Geological map of the San Felipe and San Fernando geothermal areas (modified from SGM 1999; Seiler et al., 2010). (c) Photographs of the study areas. SD: San Diego City, T: Tijuana City, SAF: San Andreas Fault, SS: Salton Sea geothermal field, CP: Cerro Prieto geothermal field, CPF: Cerro Prieto Fault, SPMF San Pedro Martir Fault, VF-SMF: Vallecitos-San Miguel fault systems, ABF- Agua Blanca Fault, MGE: Main Gulf Escarpment, SMO: Sierra Madre Occidental, CB: Cuevitas basin, CD: Cuevitas detachment, LMB: Llano El Moreno basin, SRB: Santa Rosa basin, SRD: Santa Rosa detachment, HB: Huatamote basin, HD: Huatamote detachment, PM: Punta El Machorro, SFM: San Felipe mine, SFT: San Felipe trench.

low-angle normal faults (Seiler et al., 2010; Fig. 1). Half-grabens (Cuevitas, Llano El Moreno, Santa Rosa and Huatamote; Fig. 1)

are infilled with Mio-cene–Pliocene volcanic and sedimentary rocks deposited nonconformably onto the batholithic basement (Seiler et al., 2010).

The basement is composed of Paleozoic metamorphic and metasedimentary rocks, and the Cretaceous granitic to tonalitic batholith (Ortega-Rivera, 2003). The basement is revealed in the Sierra San Felipe, Sierra Santa Rosa, Sierra San Pedro Mártir and Punta Machorro (SGM, 1999; Fig. 1). Eocene–Oligocene sedimentary sequences of sandstones, conglomerates and breccias rest unconformably on basement rocks (Oskin & Stock, 2003a). Detrital rocks from fluvial and lacustrine environments reach thicknesses of up to 400 m in structural depocenters (Seiler et al., 2010). Overlying the basal sediments are several discontinuous basalt and andesite flows, dated between ~ 21 and 19 Ma and associated with a volcanic arc (Lewis 1996; Seiler et al., 2010). The rhyolitic San Felipe Tuff overlies the Miocene lavas nonconformably, with a maximum thickness in the San Felipe region of 180 m and a $^{40}\text{Ar}/^{39}\text{Ar}$ age of 12.6 Ma (Stock et al., 1999; Oskin & Stock, 2003b).

The San Felipe Tuff and basement rocks are overlain by an extensive section of pre- to syn-tectonic basin-fill detrital rocks with intercalations of evaporites and volcanic rocks that range in age from late Miocene to early Pleistocene (Lewis, 1996; Seiler et al., 2010). Volcanic rocks include ignimbrites, ash-fall deposits, andesites, and rhyolite flows. Deposition was synchronous with slip on the basin-bounding faults and as a result, the stratigraphic record of individual basins varies considerably (Seiler et al., 2010). The youngest volcanic rocks (<3 Ma) outcrop in the southern region of the study area, south of Sierra San Felipe and comprise rhyolitic pyroclastic deposits of the San Felipe Volcanic Province (Lewis, 1996; Oskin & Stock, 2003b). The youngest strata are Pleistocene to Holocene alluvial fan, colluvium and eolian deposits that overlap the basin-bounding faults. The lithologic units that outcrop next to the hot springs consist of Paleozoic and Mesozoic metasediments from the basement.

Intertidal springs and warm wells in San Felipe are located within the coordinates: 30.7946°–31.08458°N and – 114.7845°–114.8666°W. This area is bordered to the west by the Sierra Santa Rosa and the Sierra Pedro Mártir (Fig. 2), where an important strike-slip fault conforms the limit between the batholith to the west and the alluvial deposits to the east near San Felipe. This region is characterized by low-angle normal SE-dipping faults (Amarillo, Huatamote, Santa Rosa and Cuevitas faults) that form several en echelon semi-grabens (Seiler et al.,

2010). Argillic alteration (opal, pyrite, kaolinite and native sulfur) in the area is related to fossil hydrothermal activity (Fig. 1; SGM, 1999).

Thermal intertidal vents are restricted to four sites: San Felipe, San Fernando, Punta Estrella and El Coloradito (Fig. 3). Some groundwater wells in the San Felipe Valley have temperatures of up to 34.9 °C (Table 2), which is higher than the local mean annual temperature for this area (23.6 °C); therefore, groundwater in those wells must undergo mixing with thermal water. Geochemistry data from thermal water samples near San Felipe have been reported (Landry, 1976; Lynn, 1978; Pearl, 1978; Gastil & Bertine, 1982; Álvarez, 1995; Barragán et al., 2001), and from groundwater samples from Percebú well (PRCBU; Lynn, 1978). Reported geothermometer calculations for the San Felipe and Punta Estrella samples produced temperatures ranging up to and above 200 °C (Table 5), which suggest a high enthalpy geothermal resource (Barragán et al., 2001). The reported chemical analysis of one gas sample from the San Felipe vents (Table 1; Barragán et al., 2001) was used to estimate temperatures at depth in excess of 200 °C using gas geothermometers. The geothermometry is discussed in detail in the **Results** section.

Previous Geophysical Surveys

Geophysical work in the San Felipe Valley included gravity and magnetic surveys (Slyker, 1970), the results of which suggest the predominance of regional NW-trending structures. The Curie Temperature Depth calculated with aeromagnetic data yielded a value of 8.4 ± 0.7 km, which indicates a geothermal gradient of 64–75 °C/km, more than twice the world average value (Carrillo-de la Cruz et al., 2021).

Electrical surveys that included 50 vertical electrical soundings (VES) with maximum electrode distance of 1 km were done by the local Water Authority (CONAGUA) to characterize the aquifers. These surveys defined an aquifer with very low resistivity (<10 ohm m) that was interpreted as caused by saturation with salty hot water at depths of 200–400 m and was not considered as a suitable aquifer to provide groundwater to the area (CONAGUA, 1989) but is evidence of the presence of a geothermal resource.

A magnetotelluric (MT) profile (A-A' in Fig. 4) to the north of the San Felipe Valley was done to



Figure 2. Site photographs of coastal hydrothermal vents and hydrothermal alteration. (a) Coastal hydrothermal vent area nearby San Felipe and associated alteration outcrop. (b) Intertidal hydrothermal vents in San Fernando. (c) Intermediate argillic alteration outcrop and native sulfur from veinlets from fossil hydrothermal activity in the San Felipe area. Cc: calcite, Goe: goethite, Fe: ferrihydrite, Gy: gypsum, Op: opal, Mt: montmorillonite, Kao: kaolinite, Qz: quartz, Py: pyrite, and S: native sulfur.

define the crustal structure and local tectonic evolution (Pamplona-Pérez, 2007). This survey identified a high conductivity anomaly (< 10 ohm m) that reached shallow depths to the NW of the San Felipe vents (SF 1–4 in Fig. 3). This survey suggested the presence of a geothermal system and justified detailed exploration of the whole area (Fig. 4). A NW–SE telluric–magnetotelluric (TMT) and magne-

totelluric (MT) profile (B–B' in Fig. 4) indicates an increase in resistivity at depth from the northern low resistivity anomalies detected by Pamplona-Pérez (2007) in the direction toward San Felipe and resistivity decreases again in the southernmost station toward San Fernando (González-Ávila, 2015; Ruiz-Aguilar et al., 2019).

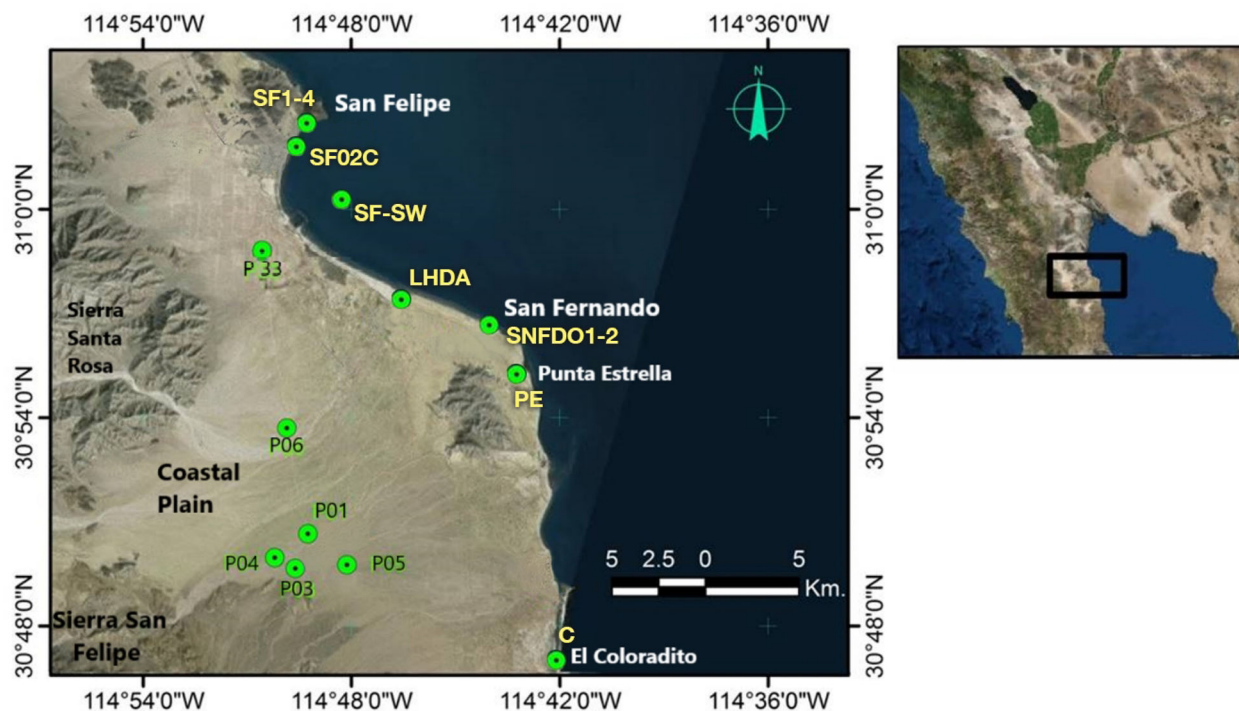


Figure 3. Location of water sampling sites (previous reports and present work) from groundwater wells and intertidal vents in the San Felipe area. Measured temperatures are shown in Table 2. SF, PE, C and SNFDO are intertidal vent samples, and the other samples are groundwater wells: LHDA, P33, P01, P03, P04, P05, and P06 that present temperatures higher than the local mean annual temperature.

Table 1. Composition of gas in San Felipe vents, concentration in mmol/mol and gas/steam ratio of 472,700 mg/kg (Barragán et al., 2001)

| Sample | CO ₂ | H ₂ S | Ar | N ₂ | CH ₄ |
|--------|-----------------|------------------|-------|----------------|-----------------|
| SF | 992 | 0.038 | 0.411 | 6.51 | 0.993 |

MATERIALS AND METHODS

Image Processing

ETM + Landsat 7 images were used to identify hydrothermal alteration minerals and main structures in the study area. Preprocessing included orthorectification, atmospheric correction and reflectance calculation. The spectral identification of hydrothermal alteration minerals was achieved with the spectral angle method that allows similitude identification between the pixel spectrum and mineral spectra from the Jet Propulsion Laboratory (JPL-NASA) spectral library (Kruse et al., 1993). The target alteration minerals were kaolinite, montmorillonite, illite, alunite, anhydrite and calcite.

Additionally, structural features were identified using digital elevation models (DEM) and geological information was obtained from the San Felipe geological map (SGM, 1999). The image processing software included Terraset and QGIS. The results of image processing applied to a multispectral image Landsat-7 ETM⁺ were correlated with features from the San Felipe H11-3 1:250,000 scale geological map and the DEM. Spatial enhancement methods (directional filters, edge enhancement; Van der Meer et al., 2014) were used to map the main lineaments in the image that were later verified during field work .

Hydrogeochemistry

The water samples from wells were collected using a Bailer sampler, and those from the intertidal vents were collected at low tide with 60 ml syringes in the discharge site. Intertidal thermal springs were discovered in a new site at San Fernando and water samples were collected there. Samples of seawater were collected as a reference on a location far from the San Felipe vents to avoid hydrothermal influ-

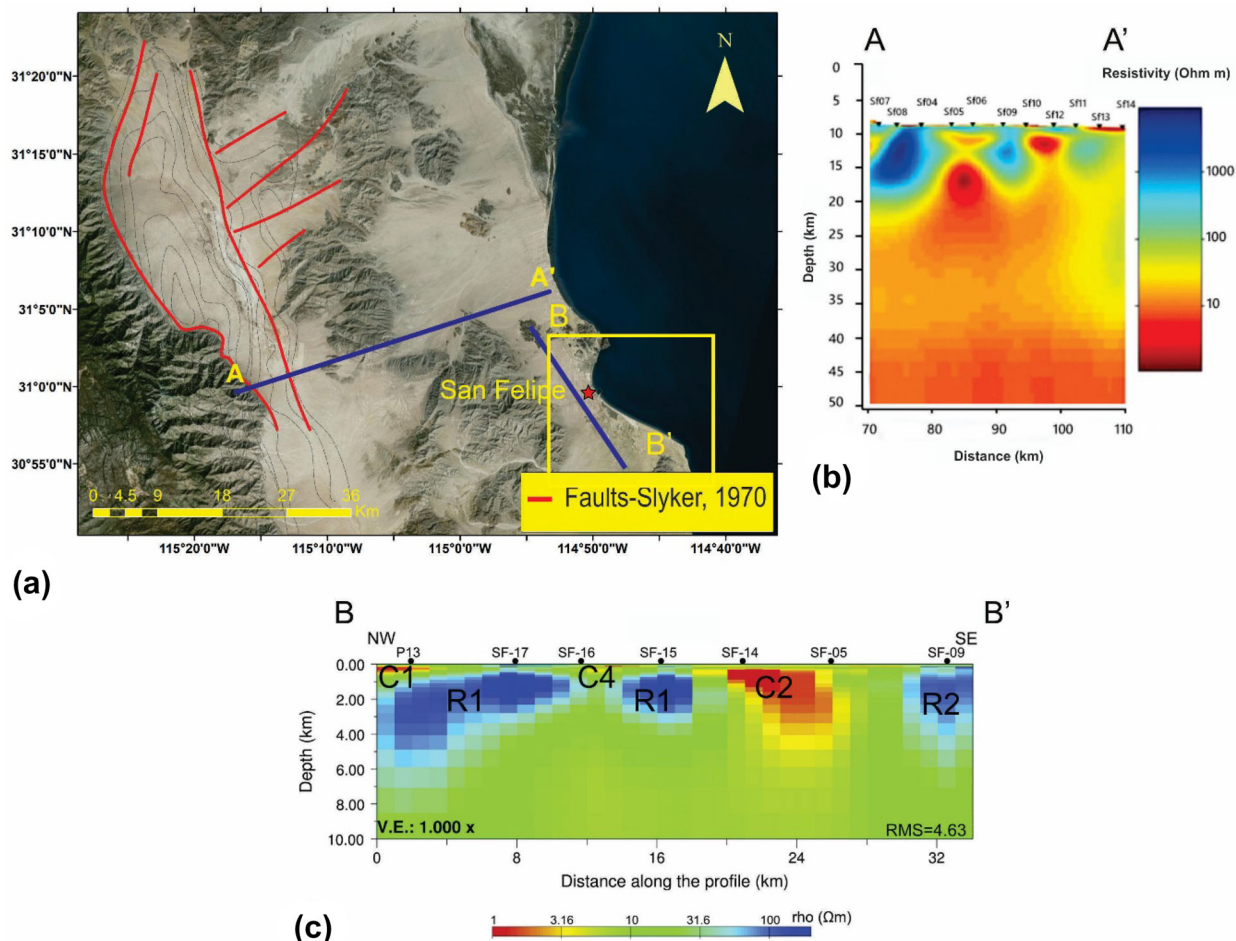


Figure 4. (a) Red lines denote structures defined by gravity and magnetic surveys, AA'—location of the MT profile shown in (b) that presents a low resistivity anomaly to the north of San Felipe Valley. (c) 2D interpretation of the MT results along the BB' profile that shows an increase in resistivity from the northern part of the San Felipe Valley toward the central and eastern part and then a further decrease. C1, C2 and C4 denote conductive bodies, R1 and R2 denote high resistivity bodies (after Slyker, 1970; Pamplona-Pérez, 2007; Ruiz-Aguilar et al., 2019). The yellow square denotes the area covered by Figure 3.

ence. In situ measurements included temperature with thermometer Oakton Acorn Series RTD, pH, alkalinity, total dissolved solids (TDS) and conductivity using a multiparameter Thermo Scientific-ORION STAR A329 with pH electrode Orion 9107BNMD, TDS and conductivity electrode Orion 013005MD. Silica and sulfate concentrations were measured in situ with a HACH@2800 equipment. Alkalinity was measured by titration. Chloride was determined with the test kit Hanna HI 3815. Chemical analysis for major cations and trace elements (B, Na, Li, Be, Mg, Al, Si, K, Ca, Sc, Ti, V, Cr,

Mn, Fe, Co, Ni, Cu, Zn, Ga, Ge, As, Se) were performed by ActLabs (analyses were performed with ICP-MS except for Na and Ca, which were analyzed with ICP-OES). Isotopic analyses were done at the Laboratorio Universitario de Geoquímica Isotópica (LUGIS-UNAM) using a Finnigan MAT 253 spectrometer with a dual inlet. The GasBench II with CO₂ equilibration method for 0.5 ml at 25 °C by continuous flow was used for measuring the oxygen isotopic ratio. Hydrogen isotopic ratio measurements were performed using a Delta Plus XL and HDevice (Werner and Brand, 2001) with the Cr

reduction method at 860 °C. $\delta^{18}\text{O}$ and δD values were normalized using VSMOW and SLAP, respectively, according to Coplen (1988). Cation geothermometers Na/K and K/Mg (Fournier, 1979; Giggenbach et al. 1983) were applied to samples that presented partial chemical equilibrium in the Na–K–Mg plot (Giggenbach, 1988). Quartz and chalcedony geothermometers (Fournier, 1977; Arnorsson, 1983) were applied to all water samples.

Geological Mapping

The geological work was planned based on the satellite multispectral image processing, focusing on the characterization of main structures and surface manifestations (warm springs, intertidal vents, warm wells and hydrothermal alteration). Rock samples were prepared for observation in a petrographic microscope and spectroscopic analysis with a spectrometer (OreXpress) in SWIR (short wavelength infrared) for identification of alteration minerals. Selected samples were analyzed by X-ray diffraction (XRD) for phase identification and examined under a scanning electron microscope (SEM).

Magnetotelluric (MT) Survey

A magnetotelluric survey was performed in the San Felipe Valley in 2014, and 13 MT soundings were measured along three profiles (Fig. 5). The acquisition of the soundings was done with Metronix ADU-07 consoles. The estimation of the apparent resistivity and phase curves was performed under the scheme of signal processing with remote reference (Goubau et al., 1978; Gamble et al., 1979) to reduce the non-correlated noise, obtaining curves in a frequency range between 1000 and 0.01 Hz.

A dimensional and directional analysis was conducted (McNeice and Jones, 2001; Caldwell et al., 2004), whereby 1D dimensionality was observed in high frequencies (1000–10 Hz) and a predominant 2D dimensionality in a frequency range of 10–0.01 Hz. Once the ambiguity of strike direction was resolved with the induction vectors (Parkinson, 1959), the electromagnetic strike directions were estimated at N42°W, N65°W and N53°W for the C–C', D–D' and E–E' profiles, respectively. Subsequently, the static shift of the soundings was corrected with TEM measurements that were made at each of the sites (Pellerin and Hohmann, 1990).

MT data inversion was performed using WinGLink software, which implements an algorithm based on nonlinear conjugate gradient inversion (Rodi and Mackie, 2001). An error floor of 5% was set for the apparent resistivity and 3° for the phase. Polarization modes TM and TE¹ were inverted together and independently. However, because the coasting effect would affect the TM mode more (Parkinson, 1962; Jones, 1992; Singh et al., 1995), it was decided to interpret the models generated from the TE mode inversion of each of the profiles. The estimated models presented RMS of 1.99, 2.78 and 2.36 for the C–C', D–D' and E–E' profiles, respectively.

Heat in Place Calculation of the Geothermal Potential

The gathered information was integrated to evaluate the geothermal potential of the southern section of the San Felipe Valley using the results of the geological, geochemical and geophysical surveys as input data for the volumetric method (Garg and Combs, 2010). This method requires estimation of three main parameters of a reservoir: volume ($A \cdot h$), reservoir temperature (T_i), and permeability. The last parameter is necessary to evaluate the recovery factor (R_f). Additionally, it is required to input the efficiency of the plant (C_e), the plant factor (P_f) and the economic life of the plant (t). The energy potential (P) is calculated with the equation:

$$P = (Q_t \cdot R_f \cdot C_e) / (P_f \cdot t)$$

where Q_t is the heat contained in the reservoir, calculated as:

$$Q_r = A \cdot h [C_{v_r} \cdot (1 - \Phi) \cdot (T_i - T_f)]$$

where C_v is the volumetric heat capacity, Φ is the porosity, and T_f is the abandonment temperature, and it depends on the selected plant. The predicted power capacity is calculated as a probability function using the Monte Carlo simulation. A rectangular probability distribution was used because only minimum and maximum values were available.

¹ An electromagnetic wave is known as TM mode (transverse magnetic mode) when the electric field vector lies in the incidence plane or it is called p-polarized, and when the electric field vector is normal to the incidence plane, it is called TE (transverse electric mode) or s-polarized.

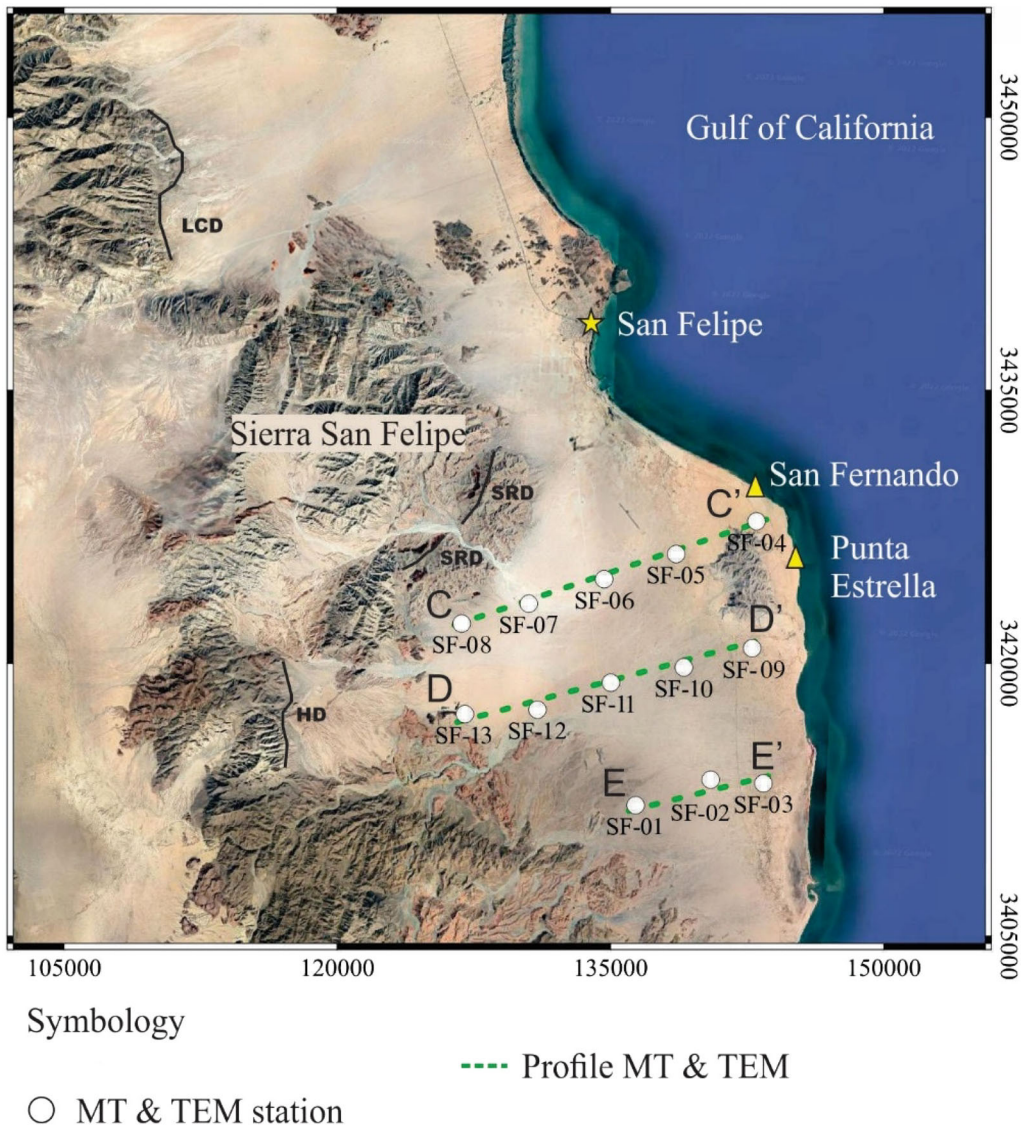


Figure 5. Location of the stations of the magnetotelluric survey along three profiles perpendicular to the coast to identify low resistivity anomalies that might be related to the presence of San Fernando and Punta Estrella coastal vents. HD = Huatamote Detachment, LCD = Las Cuevitas Detachment, SRD = Santa Rosa Detachment (Seiler et al., 2010).

RESULTS

Remote Sensing and Surface Geology

The results of image processing defined lineaments that relate to reported faults and new structures (Fig. 6). The filling of the San Felipe Valley hinders the continuation of the structures identified in the Sierras San Pedro Mártir, San Felipe, Santa Rosa and Las Pintas (Fig. 6). The predominant fault strike direction was NE–SW with an important number of faults with

NW–SE fault strike. This correlates well with previously reported structures (Lynn, 1978; Barragán et al., 2001; Seiler et al., 2010). The integration of all the reported and identified faults is presented in Figure 7. The Amarillo Fault (Seiler et al., 2010) borders the basin and it is covered by Quaternary sediments that contain the San Felipe-Punta Estrella aquifer. Alteration patches were observed in the sierras, but they were not evident in the basins and the coastal plains due to the Recent sedimentary cover that overlaps the spectral response of the geothermal alteration minerals.

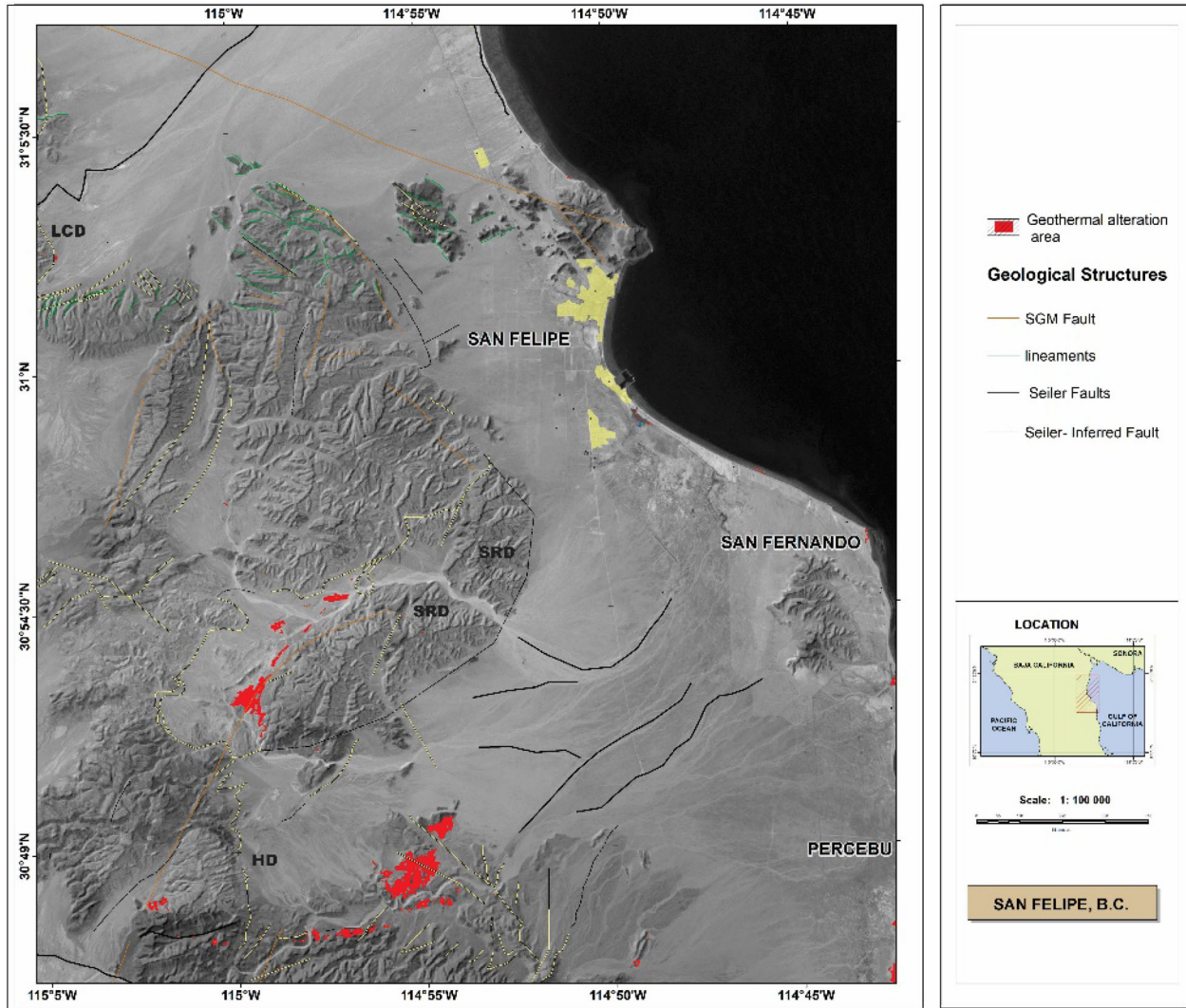


Figure 6. Results of multispectral image processing. Hydrothermal alteration areas identified using spectral enhancement of multispectral satellite images. Lineaments were identified by applying spatial enhancement to the satellite images as described in the methodology and verified in the field. Structures reported by Seiler et al. (2010) and SGM (1999) are also included. HD = Huatamote Detachment, LCD = Las Cuevitas Detachment, SRD = Santa Rosa Detachment (Seiler et al., 2010).

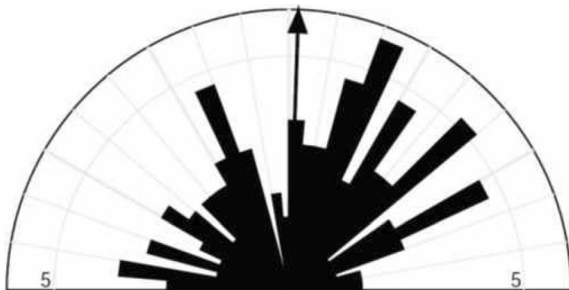


Figure 7. Rosetta diagram for San Felipe that includes all the field mapped regional faults with length > 2 km and local faults with length < 2 km, the predominant systems have NE strike directions.

The main fault strike directions were NW–SE and NE–SW, and the most recent fault system strike was N–S. These faults have typical orientations caused by the extensional regime in this region. The NE–SW-trending lineaments are concordant with the mapped detachment faults: Las Cuevitas, Santa Rosa and Huatamote.

Hydrothermal Manifestations

The area where intertidal vents discharge near San Felipe is characterized by the presence of frac-

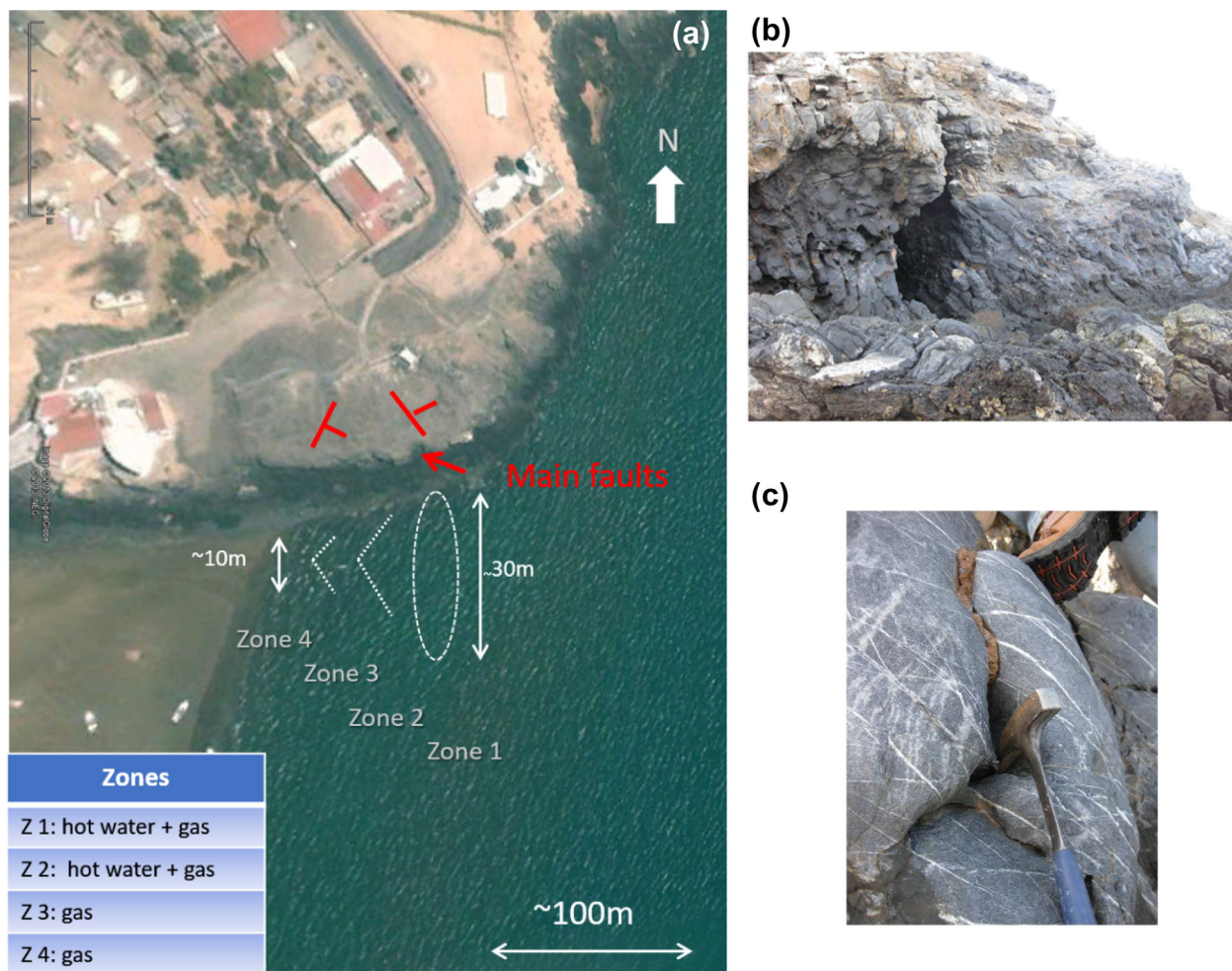


Figure 8. (a) Location of the coastal vents in San Felipe. (b) Faulted breccia outcrop on the beach where coastal vents occur. (c) Calcite and opal veins in the breccia fragments.

tures filled with hydrothermal breccias with fragments of metasedimentary rocks from 2 to 30 cm in size, which are cemented by silica and carbonate with hematite and goethite that correspond to different hydrothermal stages (Fig. 8). The breccia extends offshore down to 2.5 m depth. Normal faults are evident in the coastal outcrop with NW, NE and NS strike directions. Some calcite veins strike E–W, and the main strike direction of the breccia filling in the host rock was E-dipping, striking NW26. The veins on the breccia fragments suggest several stages of hydrothermal activity (Fig. 8c).

Intertidal vents in San Felipe and San Fernando pass almost unnoticed although they have temperatures in the range 31–74 °C (the average seawater temperature was 24 °C) but mixing with seawater masks those with the highest temperatures. There-

fore, hot springs located at San Fernando Beach had not been previously reported; they discharge hot water and gas along faults in granitic rocks. In those locations, the springs occupy areas of 900 m² and 1080 m², respectively. Fractures and faults were measured in the outcrop on the coast, the main structures related with the intertidal springs in San Fernando have strike directions NE10–26° and dips from 70° NW to subvertical. Hydrothermal minerals as pyrite, barite, opal and anhydrite occur on the intertidal springs (Fig. 9).

Hydrogeochemistry

Localization, description, and geochemical data of thermal water and groundwater are presented in

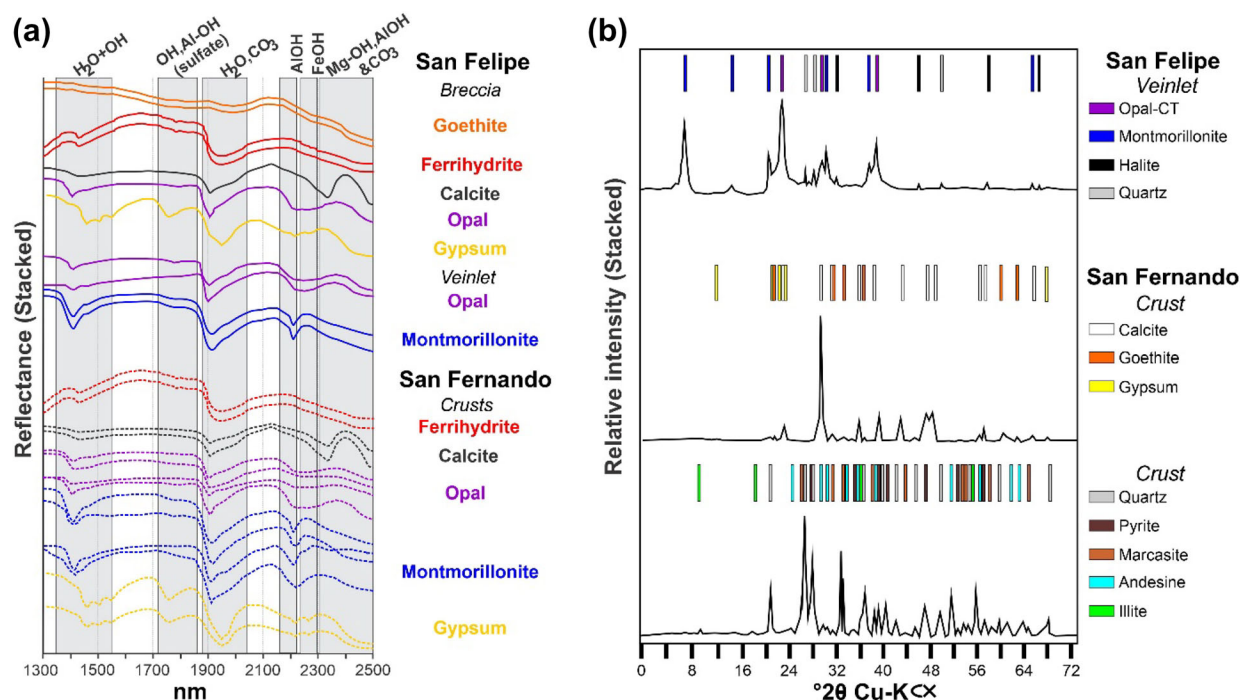


Figure 9. Mineralogy of coastal hot spring deposits and hydrothermal alteration in San Felipe geothermal area. **(a)** Short-wave infrared reflectance spectra representative of the main alteration assemblages found at San Felipe and San Fernando. The main absorption wavelengths are marked as gray bars (Clark et al., 1990). **(b)** Representative X-ray diffraction profiles of veinlets, crust and hydrothermal alteration.

Table 2. Location and sampling parameters of thermal water and groundwater in San Felipe area. (Data from: 1-Barragán et al., 2001; 2- Lynn, 1978; 3-this work)

| Sample ID | Site | N | W | T (°C) | pH |
|---------------------|---------------------------------|---------|------------|--------|-----|
| SF1 ₁ | San Felipe intertidal vents | 31.0253 | - 114.8316 | 48.0 | 5.8 |
| SF2 ₂ | San Felipe intertidal vents | 31.0253 | - 114.8316 | 50.0 | 6.3 |
| PE ₁ | Punta Estrella intertidal vents | 30.9212 | - 114.7148 | 33 | 5.8 |
| C ₁ | Coloradito intertidal vents | 30.5780 | - 114.6683 | 58.0 | 7.5 |
| LHDA ₃ | Groundwater well | 30.9568 | - 114.7762 | 25.9 | 7.9 |
| SF 02C ₃ | Groundwater well | 31.0246 | - 114.8340 | 31.4 | 7.8 |
| P01 ₃ | Groundwater well | 30.8442 | - 114.8207 | 29.5 | 7.9 |
| P03 ₃ | Groundwater well | 30.8276 | - 114.8268 | 31.9 | 7.5 |
| P04 ₃ | Groundwater well | 30.8327 | - 114.8366 | 31.6 | 7.6 |
| P05 ₃ | Groundwater well | 30.8294 | - 114.8020 | 28.1 | 8.1 |
| P06 ₃ | Groundwater well | 30.8950 | - 114.8308 | 34.9 | 8.6 |
| P33 ₃ | Groundwater well | 30.9804 | - 114.8427 | 27.1 | 7.9 |
| SF3 ₃ | San Felipe intertidal vents | 31.0258 | 114.8292 | 45.1 | 6.1 |
| SF4 ₃ | San Felipe intertidal vents | 31.0258 | 114.8292 | 46.1 | 6.1 |
| SNFDO1 ₃ | San Fernando intertidal vents | 30.9445 | 114.7336 | 33.2 | 5.7 |
| SNFDO2 ₃ | San Fernando intertidal vents | 30.9445 | 114.7336 | 33.2 | 5.9 |
| SFSW ₃ | San Felipe seawater | | | 24.5 | 8 |

Tables 2 and 3, which also included data reported from Lynn (1978) and Barragán et al. (2001) (only samples with ionic balance $\leq 10\%$ are presented in Tables 2 and 3). Samples from water wells have an alkaline pH in the range of 7.9–8.6; conversely,

samples from San Felipe and the San Fernando intertidal vents had low pH from 5.7 to 6.1. Most water samples were sodium-chloride type and only four samples plot in the mixed water type, which correspond to the groundwater wells (Fig. 10).

Table 3. Chemical composition (mg/L) and ionic balance for water samples

| Sample ID | Na | K | Ca | Mg | Li | Cl | SO ₄ | HCO ₃ ⁻ | B | F | SiO ₂ | Ionic balance |
|---------------------|-------|------|------|------|----|-------|-----------------|-------------------------------|----|----|------------------|---------------|
| SF1 ₁ | 14000 | 1636 | 2411 | 222 | 27 | 27935 | 529 | 647 | 15 | 41 | 53 | - 0.9 |
| SF2 ₂ | 13550 | 1768 | 1460 | 315 | 62 | 25500 | 380 | 475 | 17 | 2 | 95 | 0.7 |
| PE ₁ | 7200 | 916 | 1943 | 69 | 17 | 15378 | 22 | 570 | 13 | 23 | 100 | - 0.3 |
| C ₁ | 2000 | 43 | 264 | 3 | 4 | 2920 | 62 | 37 | 5 | 9 | 49 | 9.5 |
| LHDA ₃ | 367 | 19 | 142 | 28 | 1 | 581 | 195 | 105 | 1 | 2 | 15 | 9.8 |
| SF 02C ₃ | 2348 | 195 | 366 | 24 | 5 | 3449 | 588 | 169 | 10 | 9 | 139 | 7.6 |
| P01 ₃ | 107 | 39 | 70 | 16 | 1 | 145 | 206 | 121 | 1 | 2 | 94 | 5.4 |
| P03 ₃ | 118 | 12 | 71 | 15 | 1 | 200 | 112 | 137 | 8 | 1 | 94 | 3.0 |
| P04 ₃ | 110 | 12 | 82 | 15 | 1 | 160 | 124 | 169 | 2 | 1 | 88 | 6.2 |
| P05 ₃ | 173 | 9 | 44 | 8 | 1 | 214 | 140 | 126 | 3 | 4 | 77 | 0.4 |
| P06 ₃ | 248 | 6 | 26 | 1 | 1 | 302 | 93 | 84 | 2 | 11 | 86 | 2.1 |
| P33 ₃ | 855 | 23 | 81 | 4 | 2 | 1260 | 186 | 132 | 2 | 8 | 192 | 1.6 |
| SF3 ₃ | 12764 | 1219 | 2016 | 500 | 21 | 24970 | 710 | 564 | 25 | 4 | 116 | 0.5 |
| SF4 ₃ | 13580 | 1352 | 2272 | 472 | 22 | 25758 | 674 | 606 | 28 | 7 | 101 | 2.3 |
| SNFDO ₁₃ | 7462 | 750 | 1717 | 87 | 16 | 12906 | 267 | 659 | 19 | 3 | 227 | 7.4 |
| SNFDO ₂₃ | 7450 | 718 | 1672 | 111 | 16 | 13366 | 111 | 659 | 17 | 1 | 194 | 5.8 |
| SFSW ₃ | 11850 | 403 | 574 | 1379 | 2 | 19227 | 2345 | 148 | 6 | 7 | 3 | 7 |

References and description of the samples as in Table 2

Isotopic analyses were performed on selected samples (Table 4) that included the San Felipe and San Fernando coastal vent samples, three samples from water wells, and a seawater sample (SFSW), also included are the isotopic concentrations from Barragán et al. (2001) and three samples from San Felipe coastal vents (SF-R1, SF-R2, SF-R3) that had been previously reported (Prol-Ledesma et al., 2010). The isotopic data are plotted in Figure 11, where the samples from the groundwater wells are close to meteoric composition and the San Felipe-San Fernando coastal vents show different $\delta^{18}\text{O}$ enrichments and a mixing pattern with seawater.

The Na, K and Mg data from Table 3 were plotted in a ternary diagram (Giggenbach, 1988) to determine the equilibrium conditions for application of cation geothermometry (Fig. 12). Water samples from the coastal vents and the groundwater wells P033 and P05 plot within the partial equilibrium zone; thus, they are suitable for calculating equilibrium temperature using cation geothermometers.

Table 5 shows the temperatures calculated with silica (Fournier, 1977; Arnorsson, 1983), and cation geothermometers for the samples that present partial equilibrium in the Na-K-Mg plot (Fig. 12) (Fournier, 1977, 1979; Arnorsson, 1983; Giggenbach et al. 1983). The low silica temperatures corroborate the effects of strong mixing with silica-poor water and the Na/K geothermometer consistently produces temperatures above 200 °C for the vent samples. The application of gas geothermometers based on the equilibrium of CO₂-Ar and CH₄-CO₂

(Giggenbach, 1991) to the reported gas concentration in San Felipe vents (Table 1; Barragán et al., 2001) delivered temperature values higher than those obtained with silica and cation geothermometers: 255 and 351 °C, respectively. The elevated temperature calculated with the CH₄-CO₂ geothermometer was associated with the slow equilibration of methane and may represent the deep conditions in the reservoir (Giggenbach, 1991).

Geophysics

The results of 2D inversion of the magnetotelluric data are shown in Figure 13, where three main structures with anomalously low (C1, C2) and high resistivity (R) can be defined. These structures are discontinuous along the three profiles, and it is evident that they deepen toward the south.

C1 structure represents a conductive body with resistivity of approximately 4 ohm-m that can be identified in all MT-sites on the profile C-C' from the surface down to depths of approximately 500 m, while in profiles D-D' and E-E' it is present only in sites SF9 and SF11 and from sites SF01 to SF03, respectively. A second conductive body ~ 8 ohm-m (C2) extends at depth on profile C-C' from the site SF06 toward the west, and from ~ 2 km down on profile D-D' from site SF11. However, along E-E' profile it is not so evident, and it might be associated with an inductive effect of the structure present in profiles C-C' and D-D' (Ledo et al., 2002).

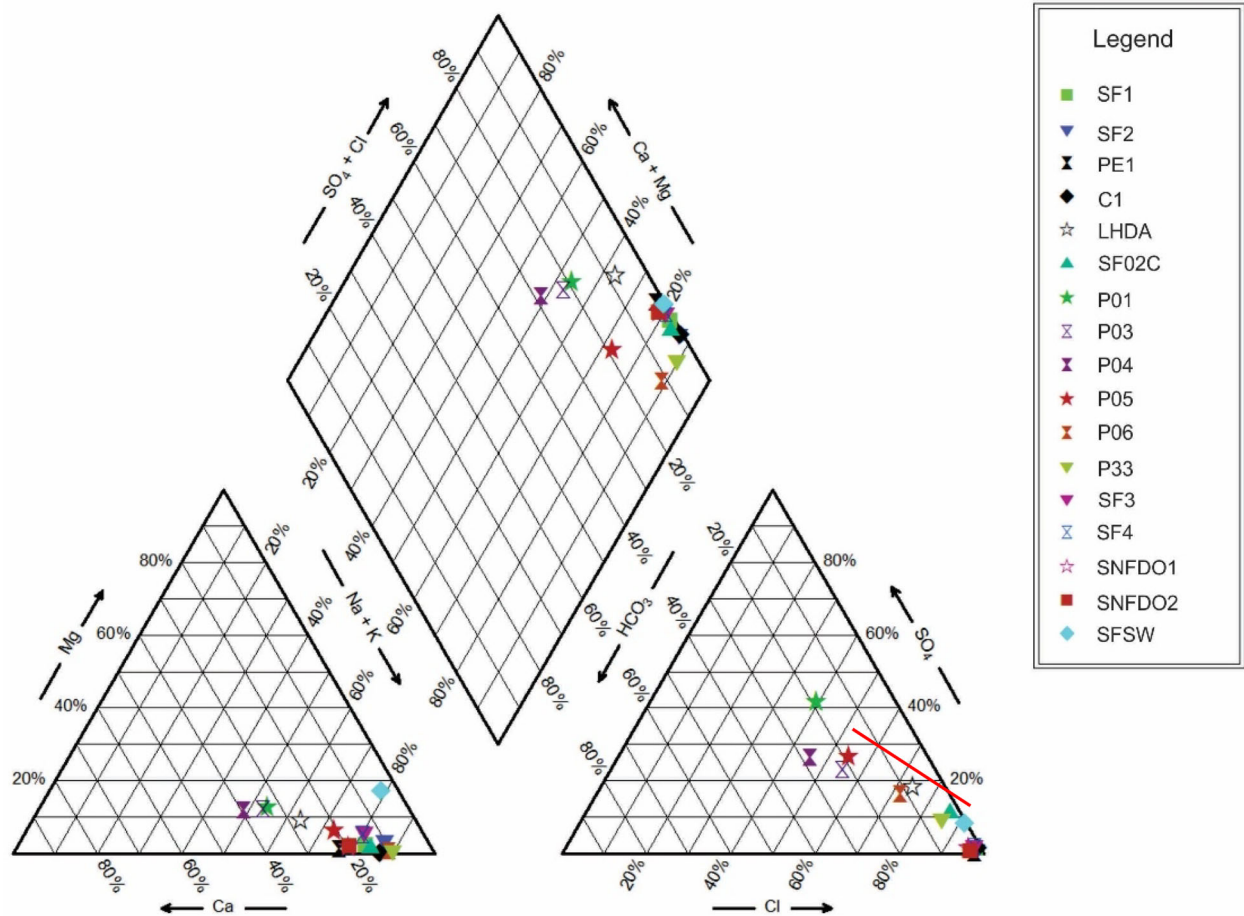


Figure 10. Piper diagram including water samples from hydrothermal manifestations, seawater and groundwater wells (see Table 2 for sample description) of San Felipe-San Fernando areas. Samples ID as in Table 2. The red line shows linear trend followed by anion concentrations of vent samples and seawater.

DISCUSSION

The presence of a hydrothermal system in the study area was revealed by an MT survey that was part of a regional tectonic research. After the presence of high conductivity anomalies was confirmed, further evidence of the presence of a geothermal resource was added by the occurrence of hydrothermal vents and hot groundwater wells in the San Felipe, San Fernando, Punta Estrella and Coloradito areas that are related to structures that may be the continuation of the Agua Blanca and San Miguel regional right-lateral faults, and to the Las Cuevitas, Santa Rosa and Huatamote detachment faults (Seiler et al., 2010). These conjugate fault systems (NW–SE- and NE–SW-trending normal faults) and fractures (Seiler et al., 2010) may operate as conduits for hydrothermal fluids to reach the

surface off the coast at San Felipe and San Fernando. The breccia outcrop related with the main coastal vents in San Felipe reveals that the hydrothermal discharge occurs at the intersections of NW-, NE-, and N–S-trending faults. The main strike direction of the breccia filling was S26E and the petrography suggests diverse hydrothermal stages in the area, which point to a long-lived hydrothermal system.

The geochemical characteristics of the thermal water from the vents and wells show the predominance of Na–Cl waters that follow a mixing pattern from the seawater and coastal vents to the groundwater well samples that have high content of sulfate and bicarbonate (Fig. 10). However, this mixing pattern is qualitative and cannot be quantified to establish the amount of each end member present in the samples because the linear regression of the

Table 4. Isotopic composition of selected water samples from San Felipe area

| Sample ID | $\delta^{18}\text{O}_{\text{VSMOW}} \text{‰}$ | $d\text{D}_{\text{VSMOW}} \text{‰}$ |
|---------------------|---|-------------------------------------|
| SF1 ₁ | - 1.8 | - 38 |
| PE ₁ | - 5.8 | - 63 |
| C ₁ | - 8.3 | - 67 |
| SF-R2 ₄ | - 0.5 | - 13.9 |
| SF-R3 ₄ | - 2.1 | - 42 |
| SF-R4 ₄ | - 1.7 | - 35.1 |
| SFSW ₃ | 0.3 | 1.9 |
| P05 ₃ | - 10.3 | - 72.1 |
| P06 ₃ | - 10.7 | - 78.8 |
| P33 ₃ | - 9.5 | - 73.2 |
| SF3 ₃ | - 2.4 | - 40.7 |
| SF4 ₃ | - 2.4 | - 43.3 |
| SNFDO1 ₃ | - 6.2 | - 65.5 |
| SNFDO2 ₃ | - 5.9 | - 62.2 |

SF = San Felipe, PE = Punta Estrella, C = Coloradito, P = groundwater well, VNTSF = San Felipe coastal vents, SNFDO = San Fernando coastal vents, SFSW = San Felipe seawater. (References: 1 = Barragán et al., 2001; 3 = this work; 4 = Prol-Ledesma et al., 2010)

major ions concentration with Mg does not yield a regression coefficient higher than 0.8; therefore, there may be other processes that the thermal fluid undergoes before discharging on the coast.

The Cl/B ratio presents a clear difference between the samples from San Felipe (> ~ 1000) and the San Fernando–Punta Estrella samples (> ~ 600) with significantly higher values for the San Felipe samples. Therefore, the differences in the chemical and isotopic composition of the samples from the San Fernando and Punta Estrella vents with the San Felipe vents suggest that fluids may correspond to different reservoirs or that the fluid in San Felipe has undergone different processes during the ascent to the surface. The differences were also confirmed by the suggested different paths (oxygen shift and mixing) in the isotopic composition of water samples from San Felipe and San Fernando vents (Fig. 11). Boiling processes are discarded as a cause for the high concentration of most ions in San Felipe because boiling produces an increase in most ions and

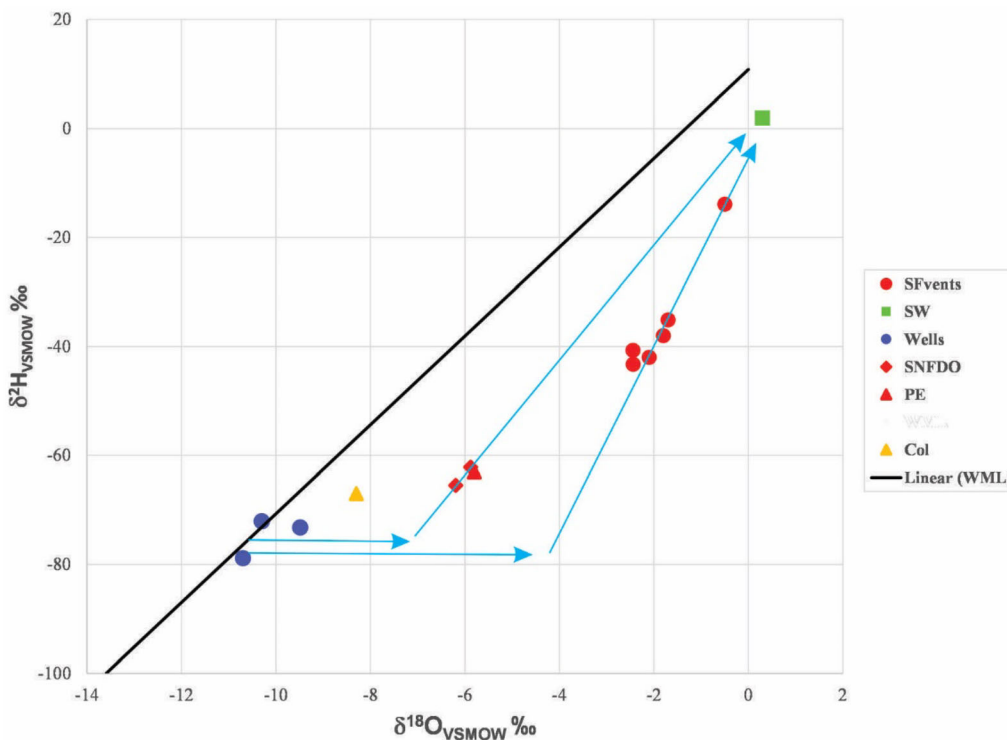


Figure 11. Isotopic composition of water samples from the San Felipe—San Fernando area. SF = water from coastal vents (SF1, SF3, SF4, SF-R1, SF-R2, SF-R3); SW = seawater without mixing with vent water (SFSW); P = groundwater wells (P05, P06, P33); SNFDO = San Fernando coastal vents (SNFDO1, SNFDO2); PE = Punta Estrella coastal vent; Col = Coloradito coastal vent; WML = World Meteoric Line. The blue arrows denote possible differences in the $\delta^{18}\text{O}_{\text{VSMOW}} \text{‰}$ enrichment of the San Felipe and San Fernando vent water before mixing with seawater.

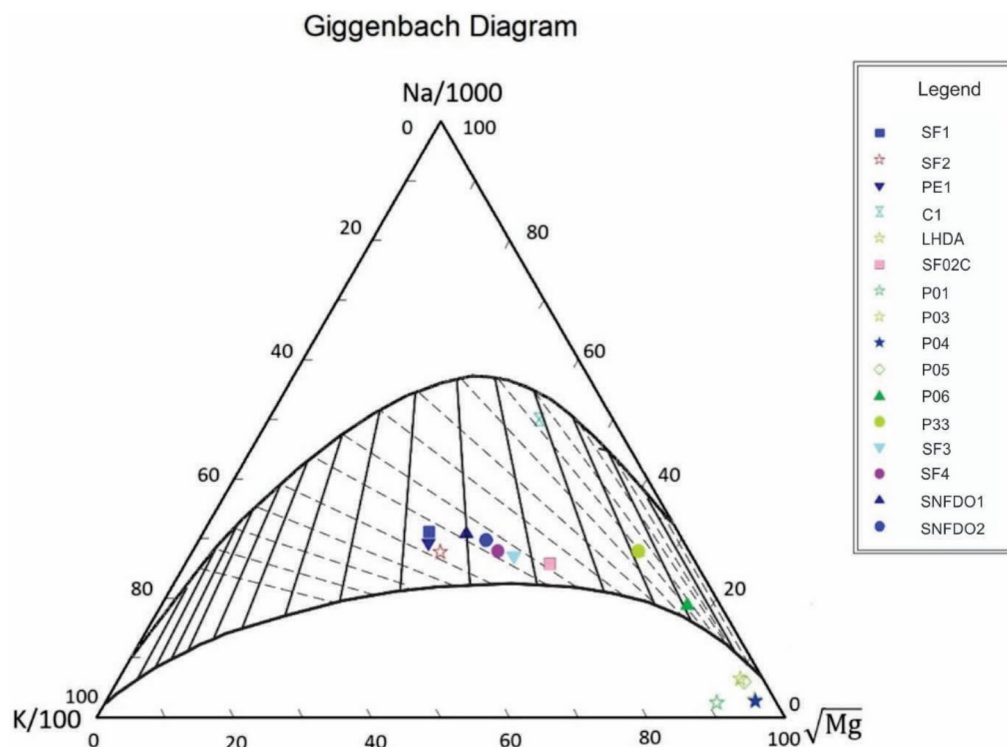


Figure 12. Na–K–Mg plot (Giggenbach, 1988) used to evaluate the equilibrium state of the thermal water for application of cation geothermometers.

Table 5. Geothermometer calculations: silica geothermometer applied to all samples and Na/K and K–Mg geothermometers applied to water samples that present partial equilibrium

| Sample number | Fournier (1977) T(Si) quartz | Arnorsson (1983) T(Si) chal- cedony | Fournier (1979) T(Na/K) | Giggenbach et al. (1983) T(K/Mg) |
|---------------------|------------------------------------|---|----------------------------|-------------------------------------|
| SF1 ₁ | 105 | 76 | 240 | 174 |
| SF2 ₂ | 134 | 106 | 251 | 170 |
| PE1 ₁ | 137 | 109 | 248 | 174 |
| C1 ₁ | 101 | 72 | 119 | 125 |
| LHDA ₃ | 52 | 24 | 173 | 70 |
| SF 02C ₃ | 157 | 129 | 210 | 137 |
| P01 ₃ | 134 | 105 | OPE | OPE |
| P03 ₃ | 134 | 106 | OPE | OPE |
| P04 ₃ | 130 | 102 | OPE | OPE |
| P05 ₃ | 123 | 95 | OPE | OPE |
| P06 ₃ | 129 | 100 | 129 | 84 |
| P33 ₃ | 177 | 150 | 130 | 99 |
| SF3 ₃ | 146 | 118 | 222 | 148 |
| SF4 ₃ | 138 | 110 | 226 | 152 |
| SNFDO1 ₃ | 189 | 162 | 226 | 162 |
| SNFDO2 ₃ | 178 | 151 | 223 | 156 |

OPE denotes water samples that plot off the partial equilibrium zone. (References and description of the samples as in Table 2)

bicarbonate concentration is similar in all vent samples, in contrast to the expected change in bicarbonate concentration as a result of boiling. Consequently, the hypothesis of two reservoirs with different chemical characteristics is more feasible.

The best correlation (99%) was obtained for the δD vs Mg plot (Fig. 14a). The δD isotopic composition of the water samples show a trend from groundwater to vent water and seawater, and the trend for $\delta^{18}O$ was distorted by the oxygen shift typical of geothermal water and it was present in the thermal water from San Fernando, Punta Estrella and the San Felipe vents that revealed a stronger interaction with the reservoir rocks in San Felipe (Fig. 14). The thermal water from the Coloradito vents presents a predominant meteoric water in contrast to the San Fernando, Punta Estrella and San Felipe vents. The San Fernando and the Punta Estrella thermal water samples were chemically and isotopically similar, suggesting that they have a common reservoir and have followed similar paths in their ascent to the surface. However, the San Felipe vents isotopic composition showed a higher component of local seawater, but their chloride

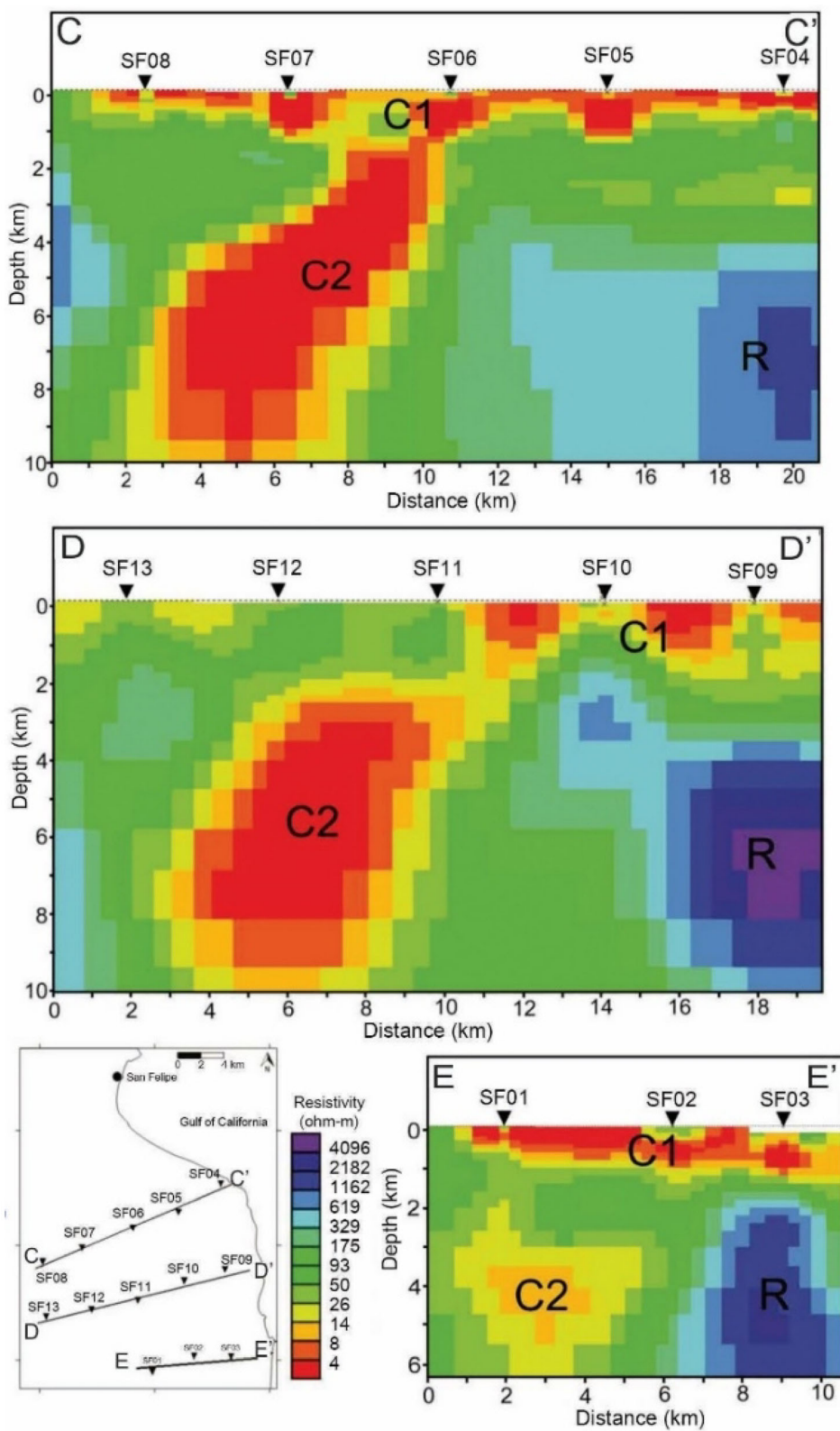
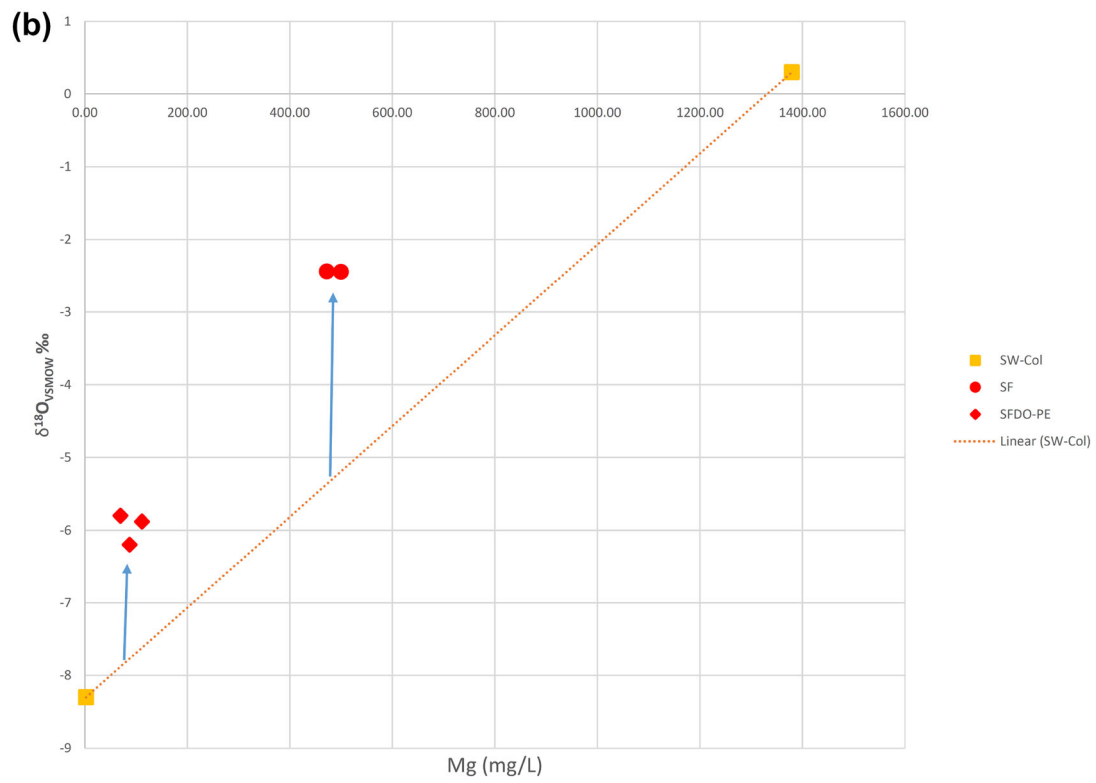
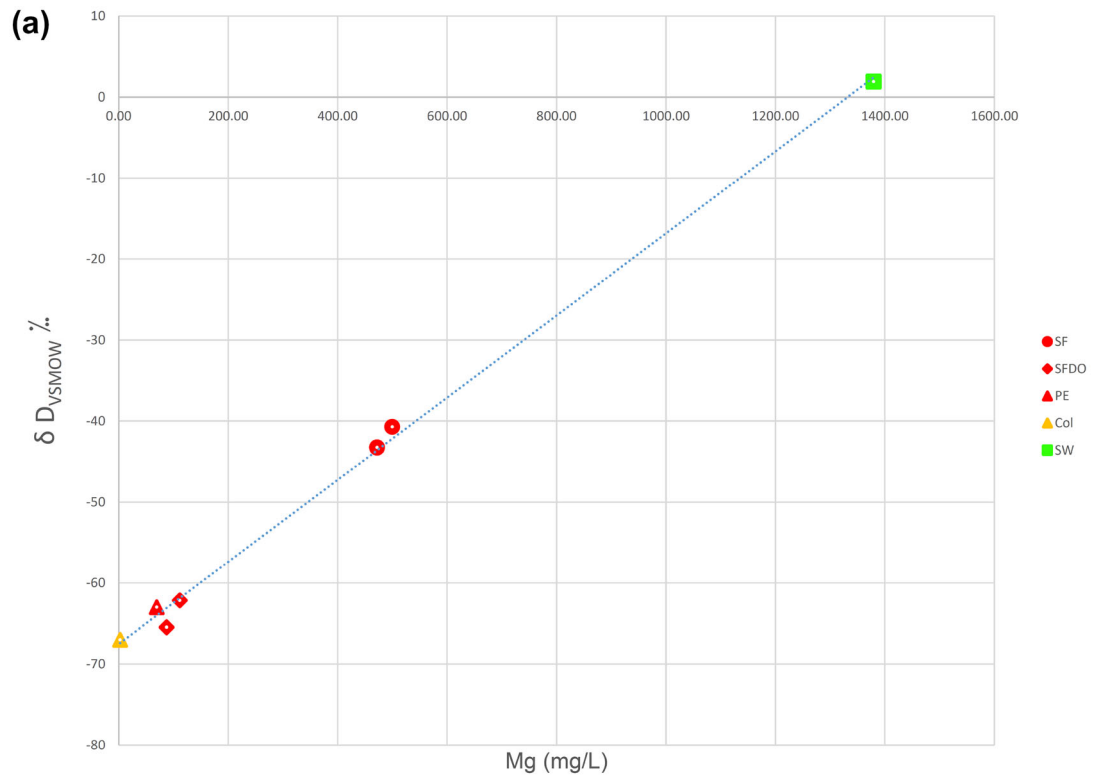


Figure 13. MT profiles that show the presence of a shallow C1 conductive body (~4 Ω.m) and a deeper C2 conductive body (~8 Ω.m).



◀ **Figure 14.** (a) δD vs Mg and (b) $\delta^{18}O$ vs Mg plots for the geothermal vents in San Felipe, San Fernando, Punta Estrella. The arrows in (b) point the $\delta^{18}O$ enrichment of the thermal water discharged by the San Felipe and San Fernando coastal vents related with isotopic exchange with the rocks. The linear trend end-members correspond to seawater and Coloradito coastal vent that represents meteoric water.

concentration was approximately 30% higher and their magnesium concentration was about one third of that of seawater. The high chloride content of the San Felipe vent water has been interpreted as chloride excess due to evaporite dissolution (Barragán et al., 2001); however, a similar increase in sulfate concentration would be expected because the evaporite dissolution process is dominated by the dissolution of $CaSO_4$ with a good correlation between Cl and SO_4 (Acero, et al., 2013; Calligaris et al., 2019); in contrast, the sulfate concentration measured in the vent samples can be explained solely by mixing with sea water (SO_4 vs Mg, $R = 98\%$) and do not present a good correlation with Cl (SO_4 vs Cl, $R = 67\%$).

Silica temperatures are affected by mixing and the calculated temperature was below $150\text{ }^\circ\text{C}$ for most samples (Table 5). The silica geothermometer yielded a temperature that was lower than that calculated with the cation and gas geothermometers probably as a result of mixing between geothermal fluids and groundwater that decreases the silica content. In contrast, groundwater mixing does not affect the results of Na/K and the gas geothermometers.

The partial equilibrium shown by vent samples supports the use of cation geothermometers. The Na/K geothermometer indicated temperatures in the range of $200\text{--}250\text{ }^\circ\text{C}$, the maximum value was similar to the temperature obtained with the $CO_2\text{--}Ar$ geothermometer of $255\text{ }^\circ\text{C}$. The temperature calculated with the $CH_4\text{--}CO_2$ geothermometer of $351\text{ }^\circ\text{C}$ suggests the presence of a deep high temperature reservoir.

Geophysical models showed a shallow conductive body (C1) associated with the alluvium that forms the San Felipe–Punta Estrella aquifer that was identified in previous studies of the sedimentary filling of the San Felipe Valley (CONAGUA, 1989). The results of the electromagnetic survey revealed the presence of a significant conductive anomaly

(C2) clearly identified in two MT profiles (stations 6 and 7 in profile C–C', and stations 11 and 12 in profile D–D') in the coastal plain of San Felipe; this anomaly (red circle in Figure 15) could point to the location of a geothermal reservoir because it extends to the south where groundwater wells (P01, P03, P04, P05, and P06 in Figure 3, shaded area in Figure 15) present anomalous temperatures of $30\text{--}35\text{ }^\circ\text{C}$ (local mean annual temperature $23.6\text{ }^\circ\text{C}$) and the silica geothermometer calculated for the groundwater samples was $123\text{ }^\circ\text{C}$.

The extension of the C2 anomaly reported here is more consistent with the temperature anomaly observed in the groundwater wells than the low resistivity anomaly reported previously (Ruiz-Aguilar et al., 2019) that is restricted to the location of only one warm well (P06) and excludes five warm wells (yellow circle in Fig. 15), and the extension of this anomaly can be considered as a minimum value for the reservoir area.

The C2 anomaly is not connected to the conductive body identified to the northwest of the San Felipe vent location (green circle in Fig. 15); moreover, the high conductivity observed to the north of San Felipe is detached from the C2 anomaly by a high resistivity body (Fig. 4c). These two highly conductive bodies (green circle and red circle) may represent two geothermal reservoirs corresponding the San Felipe hydrothermal system and the San Fernando–Punta Estrella hydrothermal system, this last shown in the cross section along the C–C' MT profile (Fig. 16), where the reservoir associated with the C2 anomaly seems to be hosted by the batholithic basement. The heat source that generates the hydrothermal activity is not clear as the most recent volcanic activities are 12.9 Ma old (San Felipe tuff) and 6.7 Ma old the air fall tuff (Seiler et al., 2010).

The San Felipe and San Fernando hydrothermal systems are located on normal faults along the eastern margin of the Santa Rosa and Huatamote basins (Fig. 16), respectively. The NW–SE- and NE–SW-trending normal faults are pathways for the fluid flow to the surface off the coast of San Felipe and San Fernando. The geological field observations and interpretations of MT results show that thermal water upflow is related to the normal faults on the hanging wall of the detachment faults (Fig. 16b). Strike-slip and detachment regional faults favor the deep circulation of meteoric waters and the upflow



Figure 15. Location of the profiles with the presence of low resistivity anomalies. The green circle denotes the low resistivity anomaly shown in the MT profile to the north of San Felipe (Pamplona-Pérez, 2007). The yellow circle shows the area covered by the C2 low resistivity anomaly identified by (Ruiz-Aguilar et al., 2019) and the red circle shows the C2 anomaly identified in this work that coincides with the warm wells location (shaded area). HD = Huatamote Detachment, LCD = Las Cuevitas Detachment, SRD = Santa Rosa Detachment (Seiler et al., 2010).

of the thermal fluids along normal fault zones in a convection dominated system (Fig. 16).

EVALUATION OF THE GEOTHERMAL RESOURCE

A conservative volumetric evaluation of the geothermal resource in the San Felipe area is re-

stricted to the estimation of maximum and minimum values of the volume and temperature due to the limited geochemical and geophysical data (Table 6). Nonetheless, an approximate evaluation of the energy potential would emphasize the importance of the future development of this energy source. The volumetric calculation was performed exclusively for the area covered by the reprocessed MT-TEM data (Fig. 13); the previously reported area to the

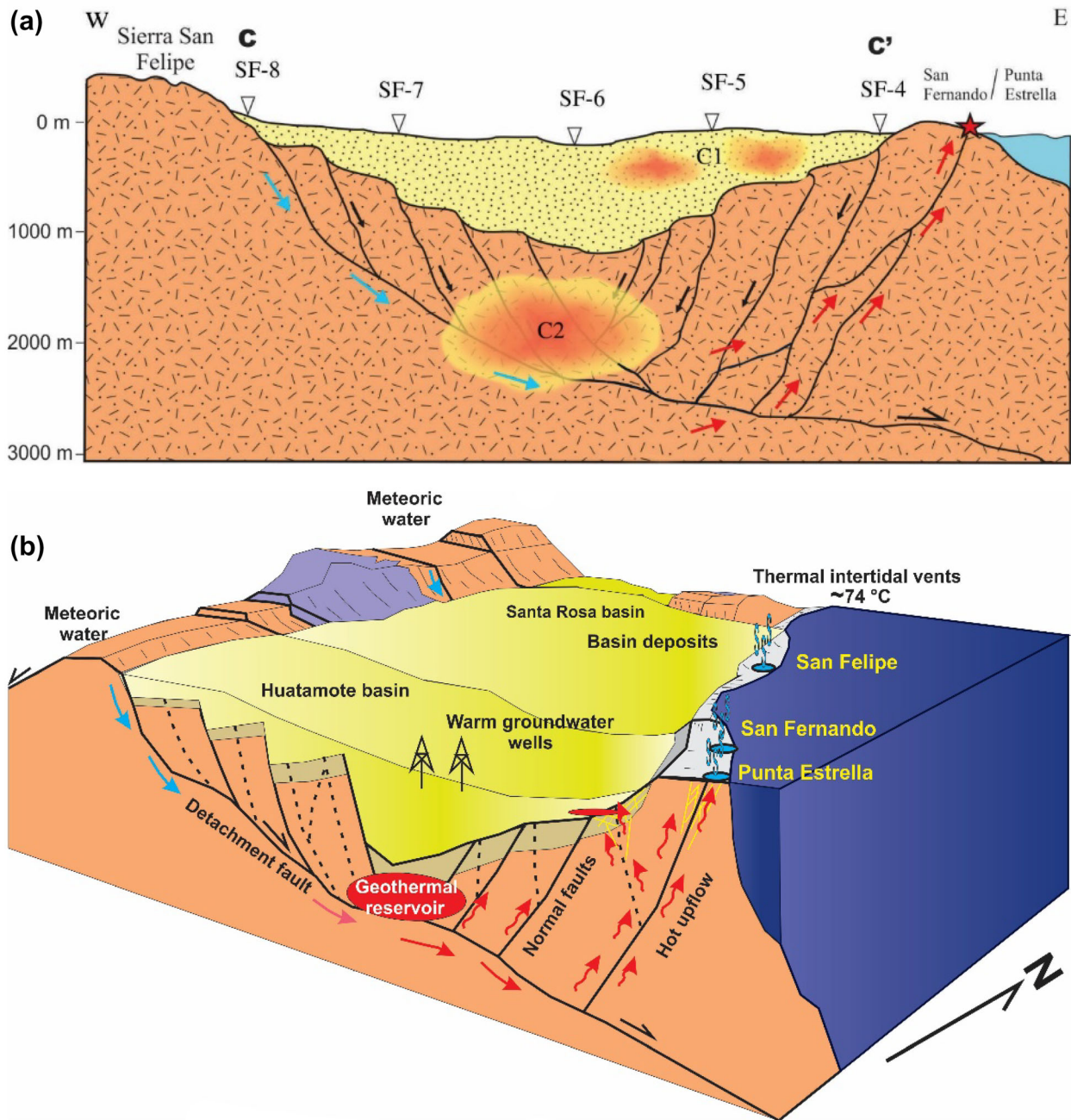


Figure 16. (a) Cross section along the MT profile C–C' from Figure 13, which shows the section of the low resistivity anomaly C2 that coincides with intense fracturing (Seiler et al., 2010) and may be considered as indication of the geothermal reservoir. The star denotes the costal vents in the southern part of the San Felipe Valley. The C1 low resistivity anomaly is related to shallow aquifers (CONAGUA, 1989). (b) Conceptual model of the San Felipe–San Fernando–Punta Estrella hydrothermal systems.

north from San Felipe (Pamplona-Pérez, 2007) was excluded in the calculation because the extension of the low resistivity anomaly cannot be constrained, as there is only one MT profile. The volume estimation

considered the results of the geophysical surveys that show the presence of the low resistivity anomaly (C2) that agree in location for both processing methods (Ruiz-Aguilar et al., 2019, and this work),

Table 6. Parameters used in the evaluation of the geothermal resource

| Parameters for San Felipe-San Fernando geothermal prospect | Min | Max |
|--|------|------|
| Area (km ²) | 17 | 32 |
| Thickness (m) | 500 | 1200 |
| Temperature (°C) | 222 | 350 |
| Volumetric rock heat capacity (kJ/m ³ °K) | 2700 | 2700 |
| Porosity | 0.05 | 0.05 |
| Thermal recovery factor | 0.05 | 0.05 |
| Abandonment temperature (°C) | 130 | 130 |
| Conversion efficiency (%) | 0.45 | 0.45 |
| Plant life (years) | 25 | 25 |
| Plant capacity factor (%) | 0.90 | 0.90 |

but the areal extension was different (Fig. 15). The smallest low resistivity area extended over an approximate area of 17 km² area (yellow area in Fig. 15) and the extension of the resistivity anomaly that contained all warm wells had an approximate area of ~ 32 km² (red area in Fig. 15). The shallow aquifer thickness of 100 m was well defined by hydrogeological studies (CONAGUA, 1989); but the thickness of the geothermal reservoir was not well constrained by the geophysical data, and the best approximation considered the scheme by Johnston et al. (1992) and Cumming (2009) to evaluate MT results, where the hydrothermal reservoir was characterized by low resistivities (10-60-Ω m). The 3D resistivity model by Ruiz-Aguilar et al. (2019) was used to evaluate the minimum thickness, and the maximum depth was linked to the detachment structures mapped by Seiler et al. (2010). A minimum thickness of approximately 500 m and a maximum of 1200 m were estimated for the volume calculation.

The temperature calculated with Na-K geothermometer for the thermal water samples was within the range of 222–251 °C, and the CH₄-CO₂ geothermometer that was expected to equilibrate slowly yielded a temperature of 350 °C that might better represent deep temperature. Therefore, the minimum and maximum temperatures were assumed to be 222 °C and 350 °C, respectively. The assumption that the reservoir is hosted by the highly fractured granodioritic basement defines the maximum porosity and the recovery factor to a maximum of 5% (Table 6). The abandonment temperature and plant efficiency were assumed to be similar to those in the Cerro Prieto installed plants (DiPippo, 2012) (Table 7).

Table 7. Megawatt capacity calculated as a Function of Probability for the San Fernando-Punta Estrella geothermal prospect

| Probability | MW capacity |
|-------------|-------------|
| 90% | 125 |
| 50% | 378 |
| 10% | 628 |

CONCLUSIONS

The San Felipe area is representative of a previously unrecognized geothermal system that was discovered by a tectonic survey, which stimulated further surveys that provided evidence of a high temperature hydrothermal system that can produce relevant amounts of energy. The geophysical and geochemical data suggest the occurrence of two separate reservoirs: one that feeds San Felipe system, and a second one that discharges at the San Fernando and Punta Estrella coastal vents.

The evaluation of the energy potential of the San Fernando and Punta Estrella demonstrate the importance of the geothermal resources of the Baja California Peninsula. The electricity demand of Baja California was less than 2,000 MW, and the contribution to the electricity requirements of Baja California by the San Felipe geothermal systems, in addition to the energy produced by Cerro Prieto geothermal field, would reach approximately 40% of the electricity demand in the state that could be provided by clean sources.

ACKNOWLEDGMENTS

Authors thank Diego Ruíz-Aguilar and Claudia Arango-Galván for their assistance during the field work. We thank the UNAM laboratories: Laboratorio de Petrografía y Microtermometría de Inclusiones Fluidas, Instituto de Geofísica, Laboratorio de Isótopos Estables and the Laboratorio Nacional de Geoquímica y Mineralogía, Instituto de Geología, especially Dr. Teresa Pi Puig for her assistance in the XRD analyzes. Isotopic analyses of water samples were performed by E. Cienfuegos and F. Otero. This work was supported by Secretaría de Energía de México and Consejo Nacional de Ciencia y Tecnología through the Project SENER-CONACYT 152823 “Evaluación de los recursos

geotérmicos de la Península de Baja California: continentales, costeros y submarinos”.

DATA AVAILABILITY

The datasets generated during and/or analyzed during the current study are available from the corresponding author on reasonable request.

DECLARATIONS

Conflict of Interest The authors declare no conflict of interest and no competing financial interests and funding.

OPEN ACCESS

This article is licensed under a Creative Commons Attribution 4.0 International License, which permits use, sharing, adaptation, distribution and reproduction in any medium or format, as long as you give appropriate credit to the original author(s) and the source, provide a link to the Creative Commons licence, and indicate if changes were made. The images or other third party material in this article are included in the article's Creative Commons licence, unless indicated otherwise in a credit line to the material. If material is not included in the article's Creative Commons licence and your intended use is not permitted by statutory regulation or exceeds the permitted use, you will need to obtain permission directly from the copyright holder. To view a copy of this licence, visit <http://creativecommons.org/licenses/by/4.0/>.

REFERENCES

- Acero, P., Gutiérrez, F., Galve, J. P., Auqué, L. F., Carbonel, D., Gimeno, M. J., Gómez, J. B., Asta, M. P., & Yechieli, Y. (2013). Hydrogeochemical characterization of an evaporite karst area affected by sinkholes (Ebro Valley, NE Spain). *Geologica Acta: an international earth science journal*, *11*(4), 389–407.
- Álvarez, J. (1995). *Reconocimiento geotérmico del noreste de la Península de Baja California proyecto Puertecitos. Reporte de avance*. Comisión Federal de Electricidad, Residencia General de Cerro Prieto, Residencia de Estudios, Cerro Prieto, México, 15 p.
- Arango-Galván, C., Prol-Ledesma, R. M., & Torres-Vera, M. A. (2015). Geothermal prospects in the Baja California Peninsula. *Geothermics*, *55*, 39–57.
- Arnorsson, S. (1983). Chemical equilibria in Icelandic geothermal systems—Implications for chemical Geothermometry investigations. *Geothermics*, *12*, 119–128.
- Atwater, T., & Stock, J. M. (1998). Pacific-North America plate tectonics of the Neogene southwestern United States: An update. *International Geology Review*, *40*, 375–402.
- Barragán, R. M., Birkle, P., Portugal, M. E., Arellano, G. V. M., & Alvarez, R. J. (2001). Geochemical survey of medium temperature geothermal resources from the Baja California Peninsula and Sonora, México. *Journal of Volcanology and Geothermal Research*, *110*, 101–119.
- Caldwell, T. G., Bibby, H. M., & Brown, C. (2004). The magnetotelluric phase tensor. *Geophysical Journal International*, *158*(2), 457–469. <https://doi.org/10.1111/j.1365-246X.2004.02281.x>.
- Calligaris, C., Ghezzi, L., Petrini, R., Lenaz, D., & Zini, L. (2019). Evaporite dissolution rate through an on-site experiment into piezometric tubes applied to the real case-study of Quinis (NE Italy). *Geosciences*, *9*, 298. <https://doi.org/10.3390/geosciences9070298>.
- Carrillo de la Cruz, J. L., Prol-Ledesma, R. M., & Gabriel, G. (2021). Geostatistical mapping of the depth to the bottom of magnetic sources and heat flow estimations in Mexico. *Geothermics*, *97*, 102225. <https://doi.org/10.1016/j.geothermics.2021.102225>.
- CENACE, <https://www.cenace.gob.mx/GraficaDemanda.aspx> (consulted 18-04-2023).
- Clark, R. N., King, T. V. V., Klejwa, M., Swayze, G. A., & Vergo, N. (1990). High spectral resolution reflectance spectroscopy of minerals. *Journal of Geophysical Research*, *95*, 12653–12680.
- CONAGUA. (1989). *Estudio de Evaluación de Disponibilidad y Calidad del Agua Subterránea en el Valle de San Felipe, B. C., para Abastecimiento de Agua a la Ciudad*. Comisión Nacional del Agua, Subdirección General de Infraestructura Hidráulica Urbana e Industrial, Gerencia de Estudios y Proyectos, Subgerencia de Estudios. México DF, 237 p.
- Coplen, T. B. (1988). Normalization of oxygen and hydrogen isotope data. *Chemical Geology*, *72*, 293–297.
- Cumming, W. (2009). Geothermal resource conceptual models using surface exploration data. In *Proceedings thirty-fourth workshop on geothermal reservoir engineering*, Stanford University, Stanford, CA.
- DiPippo, R. (2012). *Geothermal power plants: Principles, applications* (p. 599). Elsevier.
- Fournier, R. O. (1977). Chemical geothermometers and mixing models for geothermal systems. *Geothermics*, *5*, 41–50.
- Fournier, R. O. (1979). A revised equation for the Na/K geothermometer. *Geothermal Resources Council Transactions*, *3*, 221–224.
- Gamble, T., Goubau, W. M., & Clarke, J. (1979). Magnetotellurics with a remote magnetic reference. *Geophysics*, *44*(1), 53–68. <https://doi.org/10.1190/1.1440923>.
- Gastil, R. G. & Bertine, K. (1982). *Geochemical hydrothermal study of Baja California and Southern California*. University of San Diego, California, unpublished report, pp. 58–61.
- Gastil, R. G., Phillips, R. P., & Allison, E. C. (1975). *Reconnaissance geology of the state of Baja California*. Geological Society of America Memoir 140, 170 p.
- Giggenbach, W. F. (1988). Geothermal solute equilibria. Derivation of Na-K-Mg-Ca geothermometers. *Geochimica et Cosmochimica Acta*, *52*, 2749–2765.

- Giggenbach, W.F. (1991). Chemical techniques in geothermal exploration. In UNITAR/UNDP *handbook on application of geochemistry in geothermal reservoir development* (pp. 119–144).
- Giggenbach, W. F., Gonfiantini, R., Jangi, B. L., & Truesdell, A. H. (1983). Isotopic and chemical composition of Parbati Valley geothermal discharges, NW-Himalaya, India. *Geothermics*, 12, 199–222.
- González-Ávila, D. (2015). *Estudio geoeléctrico en el Valle de San Felipe, Baja California*. Tesis Profesional Ingeniería Geofísica. Facultad de Ingeniería, UNAM. 77 pp. 132.248.9.195/ptd2015/noviembre/0738380/Index.html.
- Goubau, W. M., Gamble, T. D., & Clarke, J. (1978). Magnetotelluric data analysis: Removal of bias. *Geophysics*, 43(6), 1157–1166. <https://doi.org/10.1190/1.1440885>.
- Gutiérrez-Gutiérrez, A., & Suárez-Vidal, F. (1988). Tectonic reconstruction of Agua Blanca fault in the Bahía De Todos Santos, Baja California, Mexico. *Ciencias Marinas*, 14(2), 15–28. <https://doi.org/10.7773/cm.v14i2.595>.
- Henry, C. D., & Aranda-Gomez, J. J. (2000). Plate interactions control middle–late Miocene, proto-Gulf and Basin and Range extension in the southern Basin and Range. *Tectonophysics*, 318(1–4), 1–26.
- Jones, A. G. (1992). Electrical conductivity of the continental lower crust. In D. M. Fountain, R. J. Arculus, & R. W. Kay (Eds.), *continental lower crust* (pp. 81–143). Elsevier.
- Johnston, J., Pellerin, L., & Hohmann, G. (1992). Evaluation of electromagnetic methods for geothermal reservoir detection. *Transactions-Geothermal Resources Council*, 16, 241–245.
- Kruse, F. A., Lefkoff, A. B., Boardman, J. W., Heidebrecht, K. B., Shapiro, A. T., Barloon, P. J., & Goetz, A. F. H. (1993). The Spectral Image Processing System (SIOS)—Interactive Visualization and Analysis of Imaging Spectrometer Data. *Remote Sensing of Environment*, 44, 145–163.
- Landry, W. R. (1976). *Reconnaissance of hot springs in Northern Baja California*. San Diego State University, Geology Department. Senior Report.
- Ledo, J., Queralt, P., Martí, A., & Jones, A. G. (2002). Two-dimensional interpretation of three-dimensional magnetotelluric data: an example of limitations and resolution. *Geophysical Journal International*, 150(1), 127–139. <https://doi.org/10.1046/j.1365-246X.2002.01705.x>.
- Lewis, C. J. (1996). Stratigraphy and geochronology of Miocene and Pliocene volcanic rocks in the Sierra San Fermín and southern Sierra San Felipe, Baja California, Mexico. *Geofísica Internacional*, 35(1), 3–25.
- Lynn, S. M. (1978). *Coastal warm spring systems along Northeastern Baja California*. Master of Science, San Diego State University. 217pp.
- Magar, V., Godínez, V. M., Gross, M. S., López-Mariscal, M., Bermúdez-Romero, A., Candela, J., & Zamudio, L. (2020). In-stream energy by tidal and wind-driven currents: An analysis for the Gulf of California. *Energies*, 13, 1095. <http://doi.org/10.3390/en13051095>.
- Mark, C., Chew, D., & Gupta, S. (2017). Does slab-window opening cause uplift of the overriding plate? A case study from the Gulf of California. *Tectonophysics*, 719, 162–175.
- McNeice, G. W., & Jones, A. G. (2001). Multisite, multifrequency tensor decomposition of magnetotelluric data. *Geophysics*, 66(1), 158–173. <https://doi.org/10.1190/1.1444891>.
- Muñoz-Meléndez, G., Díaz-González, E., Campbell-Ramírez, H.E. & Quintero-Núñez, M. (2012). *Baja California Energy Profile 2010–2020. Proposal and analysis of energy for the development of state prospectives*. USAID Report. Comisión Estatal de Energía de Baja California. Baja California, México.
- Muñoz-Andrade, D., Sweedler, A., Martin, J., Prieto, A., Rounds, K. & Gruenwald, T. (2020). *Baja California Energy Outlook 2020–2025*. Institute of the Americas.
- Ortega-Rivera, A. (2003). Geochronological constraints on the tectonic history of the Peninsular Ranges batholith: Boulder, Colorado, Geological Society of America Special Paper 374, pp. 297–335.
- Oskin, M. & Stock, J. M. (2003a). Cenozoic Volcanism and Tectonics of the Continental Margins of the Upper Delfín Basin, Northeastern Baja California and Western Sonora. In: S. E. Johnson, S. R. Paterson, J. M. Fletcher, G. H. Girty, D. L. Kimbrough, A. Martín-Barajas (Eds.), *Tectonic evolution of Northwestern México and the Southwestern USA*. Geological Society of America Special Paper, 374, pp. 421–438.
- Oskin, M., & Stock, J. M. (2003b). Pacific-North America plate motion and opening of the Upper Delfín basin, northern Gulf of California, Mexico. *Geological Society of America Bulletin*, 115(10), 1173–1190.
- Pamplona-Pérez, U. (2007). *Perfil Magnetotélurico a través de la Sierra San Pedro Mártir Baja California, México*. Tesis Maestría, Ensenada, Baja California. CICESE. 96 pp. <http://cicese.repositorioinstitucional.mx/jspui/handle/1007/2412>.
- Parkinson, W. D. (1959). Directions of rapid geomagnetic fluctuations. *Geophysical Journal International*, 2(1), 1–14. <http://doi.org/10.1111/j.1365-246X.1959.tb05776.x>.
- Parkinson, W. D. (1962). The influence of continents and oceans on geomagnetic variations. *Geophysical Journal International*, 6(4), 441–449. <https://doi.org/10.1111/j.1365-246X.1962.tb02992.x>.
- Pearl, J. E. (1978). *Deposits of sulfur hot spring along the northeast coast of Baja California*. Master of Science, San Diego State University.
- Pellerin, L., & Hohmann, G. W. (1990). Transient electromagnetic inversion: A remedy for magnetotelluric static shifts. *Geophysics*, 55(9), 1242–1250. <https://doi.org/10.1190/1.1442940>.
- Popkin, B.P. (1982). Potential Energy Resources of the Gulf of California, Northwestern Mexico. In *Proceedings of the 1982 Meetings of the Arizona Section—American Water Resources Assn. and the Hydrology Section—Arizona—Nevada Academy of Science*, 12, 75–85. <http://hdl.handle.net/10150/301310>.
- Portugal, E., Birkle, P., Barragán, R. R. M., Arellano, G. V. M., Tello, E., & Tello, M. (2000). Hydrochemical–isotopic and hydrogeological conceptual model of the Las Tres Vírgenes geothermal field, Baja California Sur, México. *Journal of Volcanology and Geothermal Research*, 101, 223–244.
- Prol-Ledesma, R. M., Arango-Galván, C., Flores-Márquez, E. L. & Villanueva-Estrada, R. E. (2010). *Energía geotérmica para desalación de agua de mar. Proyecto IMPULSA IV Desalación de agua de mar con energías renovables*. Instituto de Ingeniería, UNAM, México, D.F., 113 pp.
- Quintero-Núñez, M., Muñoz, M. G., Campbell, R. H. E., & Diaz, G. E. (2013). Towards a profile of sustainable energy in Baja California, Mexico, for 2011–2025 from an environmental perspective. *WIT Transactions on Ecology and The Environment*, 176, 81–92.
- Rodi, W., & Mackie, R. L. (2001). Nonlinear conjugate gradients algorithm for 2-D magnetotelluric inversion. *Geophysics*, 66(1), 174–187. <https://doi.org/10.1190/1.1444893>.
- Ruiz-Aguilar, D., Tezkan, B., Arango-Galván, C., & Romo-Jones, J. M. (2019). 3D inversion of MT data from northern Mexico for geothermal exploration using TEM data as constraints. *Journal of Applied Geophysics*. <https://doi.org/10.1016/j.jappgeo.2019.103914>.

- Scott, E. K., Bennett, S. E., & Oskin, M. E. (2014). Oblique rifting ruptures continents: Example from the Gulf of California shear zone. *Geology*, *42*, 215–218.
- Seiler, C., Fletcher, J. M., Quigley, M. C., Gleadow, A. J. W., & Kohn, B. P. (2010). Neogene structural evolution of the Sierra San Felipe, Baja California: Evidence for proto-gulf transtension in the Gulf Extensional Province? *Tectonophysics*, *488*, 87–109.
- SGM (Servicio Geológico Mexicano). (1999). *Carta geológica-minera de San Felipe III-3*.
- Singh, U. K., Kant, Y., & Singh, R. P. (1995). Effect of coast on magnetotelluric measurements in India. *Annals of Geophysics*. <https://doi.org/10.4401/ag-4109>.
- Slyker, R. G. (1970). *Geologic and geophysical reconnaissance of the Valle de San Felipe region, Baja California, Mexico*. Thesis for the degree of Master of Science in Geology. Faculty of San Diego State College.
- Stock, J. M., Lewis, C. J., & Nagy, E. A. (1999). The Tuff of San Felipe: an extensive middle Miocene pyroclastic flow deposit in Baja California, Mexico. *Journal of Volcanology and Geothermal Research*, *93*(1–2), 53–74.
- Suárez-Vidal, F., Armijo, R., Morgan, G., Bodin, P., & Gastil, R. G. (1991). Framework of Recent and active faulting in northern Baja California. *American Association of Petroleum Geologists Memoir*, *47*, 285–300.
- van der Meer, F., Hecker, C., van Ruitenbeek, F., van der Werff, H., de Wijkerslooth, C., & Wechsler, C. (2014). Geologic remote sensing for geothermal exploration: A review. *International Journal of Applied Earth Observation and Geoinformation*, *33*, 255–269. <https://doi.org/10.1016/j.jag.2014.05.007>.
- Werner, R. A., & Brand, W. A. (2001). Referencing strategies and techniques in stable isotope ratio analysis. *Rapid Communications in Mass Spectrometry*, *15*, 501–519.
- Wetmore, P. H., Malservisi, R., Fletcher, J. M., Alsleben, H., Wilson, J., Callihan, S., Springer, A., González-Yajimovich, O., & Gold, P. O. (2019). Slip history and the role of the Agua Blanca fault in the tectonics of the North American-Pacific plate boundary of southern California, USA and Baja California, Mexico. *Geosphere*, *15*, 119–145.